REPORT NO.
UC SESM 74-9

STRUCTURES AND MATERIALS RESEARCH
DEPARTMENT OF CIVIL ENGINEERING

NONLINEAR FINITE ELEMENT DYNAMIC ANALYSIS OF AXISYMMETRIC SOLIDS

by

S. NAGARAJAN
and
E.P. POPOV

Report to
Picatinny Arsenal, Dover, New Jersey
Contract No. DAAA 21-72-C-0727

JULY 1974

STRUCTURAL ENGINEERING LABORATORY
UNIVERSITY OF CALIFORNIA
BERKELEY CALIFORNIA

STRUCTURES AND MATERIALS RESEARCH

DEPARTMENT OF CIVIL ENGINEERING

Report No. UC-SESM 74-9

NONLINEAR FINITE ELEMENT DYNAMIC ANALYSIS OF AXISYMMETRIC SOLIDS

by

S. NAGARAJAN
Assistant Research Engineer

and

E. P. POPOV
Faculty Investigator

Report to
Picatinny Arsenal, Dover, New Jersey
Contract No. DAAA 21-72-C-0727

STRUCTURAL ENGINEERING LABORATORY
UNIVERSITY OF CALIFORNIA
BERKELEY, CALIFORNIA

JULY 1974

ABSTRACT

The subject of this investigation has been the static and dynamic analysis of axisymmetric solids taking into account both material and geometric nonlinearities. A general Lagrangian formulation forms the basis for the incremental equations of motion which are solved using direct integration methods. Solution accuracy is improved by applying equilibrium correction loads at each step. Finite element discretization is achieved through the use of quadrilateral plane stress and axisymmetric elements with incompatible modes added for improvement of the element flexural characteristics. Several numerical examples are presented to demonstrate the effectiveness of the developed computer program.

TABLE OF CONTENTS

1. INTRODUCTION

The nonlinear analysis of axisymmetric solids subjected to axisymmetric loading conditions is the subject of the present investigation. Material nonlinearities arise from consideration of elastic-plastic constitutive behavior. Geometric nonlinearities are due to large displacements and are taken into account through the use of a general Lagrangian formulation as the basis for the incremental equations of motion.

The isoparametric family of elements was used by Larsen and Popov [1], and Nagarajan and Popov [2] in earlier works which considered only the effects of material nonlinearity. Both material and geometric nonlinearities were considered by Larsen [3] and Nagarajan [4] but were restricted to the study of thin and moderately thick shells of revolution due to the use of a degenerate isoparametric shell element. The present effort is an extension of these works and employs a quadrilateral finite element (together with incompatible modes) to enable the analysis of axisymmetric solids subjected to both static and dynamic loads.

Following a brief review of the incremental virtual work expression for large deformation problems, the plasticity relations and the solution method, the finite element procedure for the quadrilateral element is presented. Finally, several sample problems are considered to illustrate the capabilities of the computer program developed.

2. THEORETICAL FORMULATION

2.1 Incremental Equations of Motion

The deformation of a three-dimensional body may be described by considering its path from an initial configuration B_o to a final configuration B. An intermediate configuration may be denoted by B_1 and a neighboring one by B_2. The incremental motion of the body from B_1 to B_2 may be studied using different modes of description depending on the choice of the configuration to be used as the reference state; in the Lagrangian mode of description adopted in this study, the initial configuration B_o is chosen as the reference state.

The incremental displacement from B_1 to B_2, with respect to a global coordinate system X_I in B_o is given by

$$\underset{\sim}{u} = {}^{2}\underset{\sim}{u} - {}^{1}\underset{\sim}{u} \tag{1}$$

where the left superscripts denote the configuration. A generic material point at position $\underset{\sim}{X}$ in B_o occupies the positions

$$\underset{\sim}{x} = \underset{\sim}{X} + {}^{1}\underset{\sim}{u} \tag{2a}$$

and

$$\overline{\underset{\sim}{x}} = \underset{\sim}{X} + {}^{2}\underset{\sim}{u} = \underset{\sim}{x} + {}^{2}\underset{\sim}{u} - {}^{1}\underset{\sim}{u} \tag{2b}$$

in B_1 and B_2, respectively. Using rectangular Cartesian coordinates, the Lagrangian strain increment between B_1 and B_2 as referred to B_o is defined as

$$2E_{IJ} = u_{I,J} + u_{J,I} + {}^{1}u_{K,I}\, u_{K,J} + u_{K,I}\, {}^{1}u_{K,J} + u_{K,I}\, u_{K,J} \tag{3}$$

where the linear and nonlinear parts $\underset{\sim}{e}$ and η , respectively, can be identified as

$$2e_{IJ} = u_{I,J} + u_{J,I} + {}^{1}u_{K,I}\, u_{K,J} + u_{K,I}\, {}^{1}u_{K,J} \tag{4a}$$

and

$$2\eta_{IJ} = u_{K,I}\, u_{K,J} \tag{4b}$$

The incremental equations of motion are derived by equating the incremental virtual work between B_1 and B_2 due to the internal stress fields to that of the externally applied tractions and body forces. Details of derivation of the Lagrangian formulation are presented elsewhere [3,4,5] and the incremental variational expression, neglecting body forces, is obtained as

$$\int_{B_0} [\rho_0\, \ddot{u}_I\, \delta u_I + (S_{IJ}\, \delta E_{IJ} + {}^{1}S_{IJ}\, \delta\eta_{IJ})]\, dV = \int_{\partial B_2} \delta u_I\, {}^{2}t_I\, d\bar{a} - \int_{B_0} (\rho_0\, {}^{1}\ddot{u}_I\, \delta u_I + {}^{1}S_{IJ}\, \delta e_{IJ})\, dV \tag{5}$$

where ${}^{2}\underset{\sim}{t}$ is the traction vector in B_2, and ∂B_2 refers to the surface of B_2 where the traction is specified; $d\bar{a}$ is the infinitesimal surface element in B_2, and dV the volume element and ρ_0 the mass density in B_0. The 2nd Piola-Kirchhoff (P-K) stress increment, $\underset{\sim}{S} = {}^{2}\underset{\sim}{S} - {}^{1}\underset{\sim}{S}$, is obtained in terms of $\underset{\sim}{E}$ through a linear transformation tensor $\underset{\sim}{C}$, i.e.

$$\underset{\sim}{S} = \underset{\sim}{C}\, \underset{\sim}{E} \tag{6}$$

Substitution of this into Eq. (5) results in a nonlinear expression and a linearized form is obtained by replacing $\underset{\sim}{E}$ by $\underset{\sim}{e}$ in Eq. (6) prior to its use in Eq. (5) and using $\delta\underset{\sim}{e}$ instead of $\delta\underset{\sim}{E}$ in the latter. Further, any lack of equilibrium that may develop due to

such a linearization during each increment is taken into account on the right-hand side of Eq. (3) wherein the virtual work due to the resisting forces, rather than that due to the traction vector in B_1, is subtracted from the virtual work doe to the traction vector in B_2.

The transformation of the integral over ∂B_2 to an integral over ∂B_0 and specialization for conservative and nonconservative loading have been discussed by Oden [5] and Larsen and Popov [6]. For a nonconservative loading of the pressure type, this integral can be written as

$$\delta W_2 = - \int_{\partial B_0} \frac{\rho_0}{\rho} \, {}^2p \, \delta u_I \left(\frac{\partial X_J}{\partial x_I} - \frac{\partial X_J}{\partial x_K} \frac{\partial X_M}{\partial x_J} \frac{\partial u_K}{\partial X_M} \right) N_J \, dA \qquad (7)$$

where ${}^2p$ is the pressure on a surface element in B_2. The second term within the parantheses gives rise to a nonsymmetric load stiffness. For most engineering applications, however, the effect of this term is small and it is neglected from further consideration, especially in view of the significant increase in computational effort involved in the solution of a set of equations with a nonsymmetric coefficient matrix.

The linearized incremental equations of motion are obtained as

$$\underset{\sim}{M} \cdot \ddot{\underset{\sim}{u}} + (\underset{\sim}{K}_0 + \underset{\sim}{K}_G) \cdot \underset{\sim}{u} = {}^2\underset{\sim}{R} - \underset{\sim}{M} \cdot {}^1\ddot{\underset{\sim}{u}} - {}^1F^R \qquad (8)$$

where the left superscripts referring to configurations B_1 and B_2 correspond to the states at times t and $t + \Delta t$, respectively. $\underset{\sim}{K}_0$ $\underset{\sim}{K}_G$ are the incremental and geometric stiffnesses, respectively, and are obtained from the linearized version of Eq. (5) as

$$\delta \underset{\sim}{u} \cdot \underset{\sim}{K}_0 \cdot \underset{\sim}{u} = \int_{B_0} C_{IJKL}\, e_{KL}\, \delta e_{IJ}\, dV \tag{9a}$$

and

$$\delta \underset{\sim}{u} \cdot \underset{\sim}{K}_G \cdot \underset{\sim}{u} = \int_{B_0} {}^1S_{IJ}\, \delta \eta_{IJ}\, dV \tag{9b}$$

${}^1\underset{\sim}{F}^R$, the internal resisting forces in B_1, and ${}^2\underset{\sim}{R}$, the externally applied loads in B_2 are evaluated using the appropriate integrals in Eqs. (5,7). The inertia forces are computed by assuming $\underset{\sim}{M}$ to be a diagonal lumped mass matrix in the finite element analysis by assigning tributary volumes to the nodal points of the finite elements. Finally, damping forces may also be taken into account in the form of mass and stiffness proportional viscous damping, viz.

$$\underset{\sim}{C}_D = a_1 \underset{\sim}{M} + a_2 {}^0\underset{\sim}{K}_0 \tag{10}$$

where ${}^0\underset{\sim}{K}_0$ refers to the incremental stiffness at time t = o and a_1, a_2 are the mass and stiffness proportional damping factors respectively. $\underset{\sim}{C}_D$ is then assumed to remain constant throughout the analysis and the incremental equations of motion are modified as

$$\underset{\sim}{M} \cdot \ddot{\underset{\sim}{u}} + \underset{\sim}{C}_D \cdot \dot{\underset{\sim}{u}} + (\underset{\sim}{K}_0 + \underset{\sim}{K}_G) \cdot \underset{\sim}{u} = {}^2\underset{\sim}{R} - \underset{\sim}{M} \cdot {}^1\ddot{\underset{\sim}{u}} - \underset{\sim}{C}_D \cdot {}^1\dot{\underset{\sim}{u}} - {}^1\underset{\sim}{F}^R \tag{11}$$

2.2 Constitutive Relations

The incremental virtual work expression given in Eq. (5) is not restricted to any particular constitutive laws of material behavior. Depending upon the type of material behavior to be considered, the appropriate stress-strain transformation tensor $\underset{\sim}{C}$ relating the increments in the 2nd P-K stresses to the Lagrangian strain increments, Eq. (6), must be obtained. In the case of isotropic linear elastic materials this tensor is given by

$$C_{IJKL} = E_{IJKL} = \mu(\delta_{IK}\,\delta_{JL} + \delta_{IL}\,\delta_{JK}) + \lambda\,\delta_{IJ}\,\delta_{KL} \qquad (12)$$

where λ and μ are the Lamé constants.

The incremental theory of plasticity using the associated flow rule, with the von Mises yield condition and either isotropic or linear kinematic hardening, is adopted as the basis for establishing the constitutive bahavior of elastic-plastic materials. The details of derivation will not be presented here and may be found in several references, notably the works of Khojasteh-Bakht [7] and Larsen [3] who assumed the infinitesimal theory to be applicable also to the special case of small strains, large rotations by using the 2nd P-K stress tensor in the undeformed configuration together with the conjugate Lagrangian strain tensor. The plastic strain increments are related to the increments in the total strains by

$$E^{P}_{IJ} = A_{IJKL}\,E_{KL} \qquad (13)$$

and the elastic-plastic stress-strain transformation tensor is obtained as

$$C_{IJKL} = E_{IJKL} - E_{IJMN}\,A_{MNKL} \qquad (14)$$

For von Mises yield condition and isotropic hardening, one can obtain [7]

$$C_{IJKL} = \mu(\delta_{IK}\,\delta_{JL} + \delta_{IL}\,\delta_{JK}) + \lambda\,\delta_{IJ}\,\delta_{KL} - 9\,\mu^2\,h\,{}^{1}\overline{S}_{IJ}\,{}^{1}\overline{S}_{KL} / \overline{\sigma}^2 \qquad (15)$$

where

$$\left.\begin{aligned} & h = 2\,(1+\nu)\,(1-\zeta)\,/\,\left(E[3-\zeta(1-2\nu)]\right) \\ & \zeta = E_t/E\ ;\quad E_t = \text{slope of uniaxial stress-strain curve} \\ & \bar{\sigma} = \sqrt{3J_2}\ ,\quad \text{the equivalent stress} \\ & {}^1\bar{S}_{IJ} = {}^1S_{IJ} - \delta_{IJ}\,{}^1S_{KK}\,/\,3\ ,\quad \text{the deviatoric stress} \\ & \text{and}\qquad \nu = \text{Poisson's ratio};\quad \lambda,\ \mu = \text{Lamé constants} \end{aligned}\right\} \tag{16}$$

The isotropic hardening rule does not account for Bauschinger effect; in fact, it predicts a negative Bauschinger effect. The kinematic hardening rule suggested by Prager [8] or the modified rule of Ziegler [9] may be used in the case of linearly hardening materials but more refined models are necessary to treat general nonlinearly hardening materials under cyclic loading or subject to the influence of severe load reversels. The linear hardening rule of Prager has been incorporated into the developed computer program. The yield surface is assumed to retain its initial shape and size and simply undergo a translation proportional to the plastic strain rate, i.e.

$${}^1\dot{\alpha}_{IJ} = c\,{}^1\dot{E}^P_{IJ} \tag{17}$$

where the function c is experimentally determined. Following [7], the elastic-plastic stress-strain transformation tensor for this case can be obtained as

$$C_{IJKL} = \mu(\delta_{IK}\,\delta_{JL} + \delta_{IL}\,\delta_{JK}) + \lambda\,\delta_{IJ}\,\delta_{KL} - 4\mu^2 h\,({}^1\bar{S}_{IJ} - {}^1\alpha_{IJ})\,({}^1\bar{S}_{KL} - {}^1\alpha_{KL}) \tag{18}$$

where

$$h = [2\,k^2\,(2\mu + c)]^{-1} \tag{19}$$

Using the uniaxial tensile test data to define k and c, one gets

$$k = \sigma_y/\sqrt{3} \quad ; \quad c = 2\,H'/3 = 2\,E\zeta/[3(1 - \zeta)] \tag{20}$$

where σ_y = yield stress and H' = slope of the $\bar{\sigma}$ - $\bar{\varepsilon}^{P}$ curve.

In addition to the constitutive relations, it is also necessary to define a loading/unloading criterion. Depending on the state of stress, the yield function f is computed and an elastic state is indicated if $f < 0$, and a plastic state if $f = 0$; $f > 0$ constitutes an inadmissible state in the theory of plasticity. Associated with the plastic state $f = 0$, three types of behavior are recognized, viz, loading, unloading and neutral loading which are characterized by $\dot{f} > 0$, $\dot{f} < 0$ and $\dot{f} = 0$, respectively.

3. FINITE ELEMENT ANALYSIS

The isoparametric family of elements [10] has been successfully used in the elastic-plastic analysis of axisymmetric solids under both static and dynamic loading [1,2]. But the use of these elements becomes computationally inefficient especially in the analysis of moderately thick shells considering both material and geometric nonlinearities. A degenerate isoparametric shell element [11] was successfully employed [3,4] and considerable economy in computational effort was achieved. However, construction of discrete models to represent thick shells or shells with sharp discontinuities in geometry such as due to cut-outs or stiffeners necessitate the use of one or more elements belonging to the isoparametric family. In this connection, it is desireable to keep to a minimum the number of degrees of freedom in the element and a quadrilateral element with two incompatible modes [12] has been chosen in this study. The incompatible displacement modes are selected to be of the same form as the errors associated with the basic isoparametric quadrilateral element. The displacement amplitudes associated with these modes are additional degrees of freedom which can be eliminated at the element level by minimizing the strain energy with respect to these amplitudes. This is equivalent to the static condensation algorithm which can be accomplished quite readily using the standard Gauss elimination technique [12]. The additional computational effort involved is far outweighed by the improvement obtained in the accuracy of the element.

3.1 Interpolation Polynomials

The geometry of a general quadrilateral element, Fig. 1, can be described using interpolation polynomials in terms of local natural coordinates (ξ, η) and the global nodal point coordinates (r_i, z_i), i.e.

$$\begin{Bmatrix} r \\ z \end{Bmatrix} = \sum_{i=1}^{4} \phi_i (\xi,\eta) \begin{Bmatrix} r_i \\ z_i \end{Bmatrix} \tag{21}$$

where the polynomials can be written down as

$$\left.\begin{aligned} \phi_1 (\xi, \eta) &= 1/4 (1 - \xi) (1 + \eta) \\ \phi_2 (\xi, \eta) &= 1/4 (1 - \xi) (1 - \eta) \\ \phi_3 (\xi, \eta) &= 1/4 (1 + \xi) (1 - \eta) \\ \phi_4 (\xi, \eta) &= 1/4 (1 + \xi) (1 + \eta) \end{aligned}\right\} \tag{22}$$

The local natural coordinates (ξ, η) of any point within the element are such that $-1 \leq \xi \leq +1$ and $-1 \leq \eta \leq +1$. The displacement field for an isoparametric quadrilateral element is specified by the same interpolation polynomials used for the geometry, i.e.

$$\begin{Bmatrix} u \\ w \end{Bmatrix} = \sum_{i=1}^{4} \phi_i (\xi, \eta) \begin{Bmatrix} u_i \\ w_i \end{Bmatrix} \tag{23}$$

where (u_i, w_i) are the global displacements of the i-th nodal point. The two incompatible modes [12] given by

$$\begin{aligned} &\phi_5(\xi, \eta) = 1 - \xi^2 \\ \text{and} \quad &\phi_6(\xi, \eta) = 1 - \eta^2 \end{aligned} \tag{24}$$

are added to the basic displacement field such that

$$\begin{Bmatrix} u \\ w \end{Bmatrix} = \sum_{i=1}^{4} \phi_i (\xi, \eta) \begin{Bmatrix} u_i \\ w_i \end{Bmatrix} + \phi_5 (\xi,\eta) \begin{Bmatrix} \alpha_1 \\ \alpha_2 \end{Bmatrix} + \phi_6 (\xi,\eta) \begin{Bmatrix} \alpha_3 \\ \alpha_4 \end{Bmatrix} \tag{25}$$

Each element then has four displacement amplitudes (α_1, α_2, α_3 and α_4 associated with the incompatible modes) in addition to the two degrees of freedom (u_i, w_i) at each nodal point.

3.2 Strain-Displacement Relations

The linear and nonlinear parts of the incremental Lagrangian strain between configurations B_1 and B_2 referred to B_0 are given by Eqs. (4a, 4b). The linear part may be rewritten as

$$2\, e_{IJ} = (\delta_{KI} + {}^1u_{K,I})\, u_{K,J} + (\delta_{KJ} + {}^1u_{K,J})\, u_{K,I} \tag{26}$$

The components of the deformation gradient ${}^1\underset{\sim}{F}$ in B_1 with regard to B_0 are defined as

$${}^1F_{IJ} = \frac{\partial x_I}{\partial X_J} = \frac{\partial}{\partial X_J}(X_I + {}^1u_I) = \delta_{IJ} + {}^1u_{I,J} \tag{27}$$

Hence the expression for the linear strain increment can be simplified to the form

$$2\, e_{IJ} = {}^1F_{KI}\, u_{K,J} + {}^1F_{KJ}\, u_{K,I} \tag{28}$$

For axisymmetric deformations, the three coordinate axes 1, 2 and 3 are identified with r, θ and z where θ refers to the circumferential direction and r, z are the global axes. Hence,

$$\left.\begin{aligned} &u_{1,2} = u_{2,1} = u_{3,2} = u_{2,3} = 0 \\ &{}^1u_{1,2} = {}^1u_{2,1} = {}^1u_{3,2} = {}^1u_{2,3} = 0 \\ &{}^1F_{12} = {}^1F_{21} = {}^1F_{32} = {}^1F_{23} = 0 \end{aligned}\right\} \tag{29}$$

Defining

$$\{e\}^T = \langle\, e_{11}\ e_{22}\ e_{33}\ 2e_{13}\, \rangle \tag{30}$$

and

$$\{u_\partial\}^T = \left\langle\, \frac{\partial u}{\partial r}\ \ \frac{u}{r}\ \ \frac{\partial u}{\partial z}\ \ \frac{\partial w}{\partial r}\ \ \frac{\partial w}{\partial z}\, \right\rangle \tag{31}$$

the expression for linear part of the Lagrangian strain increment given by Eq. (28) can be written in the matrix form

$$\{e\} = [\Lambda]\ \{u_\partial\} \tag{32}$$

where $[\Lambda]$ is a deformation gradient matrix whose components can be obtained using Eqs. (27,28) as

$$[\Lambda] = \begin{bmatrix} 1 + \frac{\partial {}^1u}{\partial r} & 0 & 0 & \frac{\partial {}^1w}{\partial r} & 0 \\ 0 & 1 + \frac{{}^1u}{r} & 0 & 0 & 0 \\ 0 & 0 & \frac{\partial {}^1u}{\partial z} & 0 & 1 + \frac{\partial {}^1w}{\partial z} \\ \frac{\partial {}^1u}{\partial z} & 0 & 1 + \frac{\partial {}^1u}{\partial r} & 1 + \frac{\partial {}^1w}{\partial z} & \frac{\partial {}^1w}{\partial r} \end{bmatrix} \tag{33}$$

or

$$[\Lambda] = \begin{bmatrix} {}^1F_{11} & 0 & 0 & {}^1F_{31} & 0 \\ 0 & {}^1F_{22} & 0 & 0 & 0 \\ 0 & 0 & {}^1F_{13} & 0 & {}^1F_{33} \\ {}^1F_{13} & 0 & {}^1F_{11} & {}^1F_{33} & {}^1F_{31} \end{bmatrix} \tag{34}$$

This transformation matrix has to be recomputed at each step, but the transformation matrix [B] relating displacement gradients $\{u_\partial\}$ to the displacements (corresponding to element degrees of freedom) remains unchanged throughout the analysis since it depends only upon the undeformed configuration, the interpolation polynomials and their derivatives. The same transformation is also valid for $\{{}^1u_\partial\}$, and the relationships are given as

$$\{u_\partial\} = [B]\ \{\hat{u}\} \tag{35}$$

and

$$\{{}^1u_\partial\} = [B]\ \{{}^1\hat{u}\} \tag{36}$$

where $\{\hat{u}\}$ and $\{{}^{1}\hat{u}\}$ are vectors consisting, respectively, of the incremental and total nodal point displacements together with the displacement amplitudes corresponding to the incompatible modes. Derivation of the displacement gradient matrix [B] is presented in Appendix A. Combining Eqs. (32,35), the linear part of the Lagrangian strain increment is obtained as

$$\{e\} = [\Lambda]\,[B]\,\{\hat{u}\} \tag{37}$$

The nonlinear part of the strain increment can be obtained from Eq. (4b) as

$$\begin{Bmatrix} \eta_{11} \\ \eta_{22} \\ \eta_{33} \\ \eta_{13} \end{Bmatrix} = 1/2 \begin{Bmatrix} (\partial u/\partial r)^2 + (\partial w/\partial r)^2 \\ (u/r)^2 \\ (\partial u/\partial z)^2 + (\partial w/\partial z)^2 \\ (\partial u/\partial r)\,(\partial u/\partial z) + (\partial w/\partial r)\,(\partial w/\partial z) \end{Bmatrix} \tag{38}$$

This can be evaluated readily once the displacement gradients $\{u_\partial\}$ have been computed using Eq. (35). However, in the development of the geometric stiffness matrix, an explicit nonlinear strain-displacement relation will be needed and can be written as

$$\begin{Bmatrix} \eta_{11} \\ \eta_{22} \\ \eta_{33} \\ \eta_{13} \end{Bmatrix} = 1/2 \begin{Bmatrix} \langle\hat{u}\rangle\,[H_{11}]\,\{\hat{u}\} \\ \langle\hat{u}\rangle\,[H_{22}]\,\{\hat{u}\} \\ \langle\hat{u}\rangle\,[H_{33}]\,\{\hat{u}\} \\ \langle\hat{u}\rangle\,[H_{13}]\,\{\hat{u}\} \end{Bmatrix} \tag{39}$$

The matrices $[H_{ij}]$ can be obtained rather simply in terms of the displacement gradient matrix [B] as

$$[H_{ij}] = [B]^T\,[\Omega_{ij}]\,[B] \tag{40}$$

where $[\Omega_{ij}]$ are null matrices except for

$$[\Omega_{11}]_{1,1} = [\Omega_{11}]_{4,4} = 1 \tag{41a}$$

$$[\Omega_{22}]_{2,2} = 1 \tag{41b}$$

$$[\Omega_{33}]_{3,3} = [\Omega_{33}]_{5,5} = 1 \tag{41c}$$

$$[\Omega_{13}]_{1,3} = [\Omega_{13}]_{4,5} = 1 \tag{41d}$$

It should be noted that these matrices $[H_{ij}]$ are also computed only once since they are directly derivable from [B] which remains unchanged throughout the analysis as mentioned earlier.

3.3 Incremental Stiffness Matrix $[K_0]$

This matrix may be obtained using Eq. (9a) together with the linear strain-displacement relation given by Eq. (37). Thus, one obtains

$$[K_0] = \int_{B_0} [B]^T [\Lambda]^T [C] [\Lambda] [B] \, dV \tag{42}$$

or

$$[K_0] = 2\pi \int_{-1}^{1} \int_{-1}^{1} [B]^T [D] [B] \, r \, |J| \, d\eta \, d\xi \tag{43}$$

where

$$[D] = [\Lambda]^T [C] [\Lambda] \tag{44}$$

The integrations are performed rather easily using either Gaussian or Simpson quadrature formulas for which the abcissas and weights may be obtained from standard mathematical tables [13]. The values of r, $|J|$ and [B] at any integration point can be obtained using the expressions developed in Appendix A, and $[\Lambda]$ is obtained from the displacement gradients using Eq. (33). The stress-strain matrix [C] can be obtained using Eqs. (12), (15) or (18) depending on the

assumed constitutive behavior.

3.4 Geometric Stiffness Matrix $[K_G]$

The nonlinear strain-displacement relation of Eq. (38) is substituted into Eq. (9b) for evaluation of this part of the element stiffness. Thus, one obtains

$$[K_G] = \int_{B_0} \Big({}^1S_{11}\,[H_{11}] + {}^1S_{22}\,[H_{22}] + {}^1S_{33}\,[H_{33}] + 2\,{}^1S_{13}\;1/2\;([H_{13}] + [H_{13}]^T) \Big)\; dV \qquad (45)$$

Defining $\langle {}^1S \rangle = \langle {}^1S_{11}\ {}^1S_{22}\ {}^1S_{33}\ \ 2\,{}^1S_{13} \rangle$

one can write

$$[K_G] = 2\pi \int_{-1}^{1} \int_{-1}^{1} \langle {}^1S \rangle \begin{bmatrix} [H_{11}] \\ [H_{22}] \\ [H_{33}] \\ 1/2([H_{13}] + [H_{13}]^T) \end{bmatrix} r\,|J|\,d\eta\,d\xi \qquad (46)$$

3.5 Element Mass and Damping Matrices

The element mass is assumed to be concentrated at the four nodal points. The cross-sectional area of the element is computed using numerical integration at the same time the element stiffness matrices are evaluated. Each node is assigned one-fourth of the total area and the tributary volume of each node per unit radian in the circumferential direction is computed by taking the product of the tributary area and the r-coordinate of its centroid. In the case of plane stress problems, the tributary volume is simply the tributary area times the element width. Knowing the element mass density, the lumped mass at each node of the element is obtained

and represents the inertia term in the element mass matrix corresponding to the two degrees of freedom at that node.

The damping matrix $[C_D]$ is obtained as given by Eq. (10) except that it should be noted that the stiffness proportional damping factor a_2 should be taken to operate on $[{}^0\overline{K}_0]$ and not $[{}^0K_0]$ where the former is obtained after static condensation has been performed on the latter to eliminate the equations corresponding to the incompatible degrees of freedom.

3.6 Consistent Nodal Forces

3.6.1 Internal Resisting Forces

The internal resisting forces acting at the nodal points of an element and corresponding to the incompatible degrees of freedom are obtained using the second term within the parantheses of the last integral in Eq. (5). Thus, one obtains

$$\{{}^1\hat{F}^R\} = \begin{Bmatrix} {}^1F^R \\ \hline {}^1F^R_\alpha \end{Bmatrix} = \int_{B_0} [B]^T [\Lambda]^T \{{}^1S\}\, dV \tag{47}$$

or

$$\{{}^1\hat{F}^R\} = 2\pi \int_{-1}^{1} \int_{-1}^{1} [B]^T [\Lambda]^T \{{}^1S\}\, r\, |J|\, d\eta\, d\xi \tag{48}$$

where $\{{}^1F^R\}$ corresponds to the nodal degrees of freedom and $\{{}^1F^R_\alpha\}$ corresponds to the incompatible degrees of freedom.

3.6.2 Externally Applied Loading

The element nodal force vector for a pressure type nonconservative loading is given by the virtual work expression in Eq. (7). At most a linear variation of the pressure can be consi-

dered on any face of the element (say, joining nodal points i and j) and the equivalent concentrated loads at i and j are computed as

$$\{^2R\} = -\int_{\partial B_0} \frac{\rho_0}{\rho} [\bar{\psi}]^T [^1F^{-1}]^T \{N\} \langle\psi\rangle \{^2p\} \, dA \tag{49}$$

where $[\bar{\psi}]$ and $\langle\psi\rangle$ define linear variation of the variables along the face i-j, i.e.

$$\begin{Bmatrix} u \\ u_\theta = 0 \\ w \end{Bmatrix} = [\bar{\psi}] \{\bar{u}\} = \begin{bmatrix} (1-\xi)/2 & 0 & (1+\xi)/2 & 0 \\ 0 & 0 & 0 & 0 \\ 0 & (1-\xi)/2 & 0 & (1+\xi)/2 \end{bmatrix} \begin{Bmatrix} u_i \\ w_i \\ u_j \\ w_j \end{Bmatrix} \tag{50}$$

$$^2p = \langle\psi\rangle \{^2p\} = \langle(1-\xi)/2 \quad (1+\xi)/2\rangle \begin{Bmatrix} ^2p_i \\ ^2p_j \end{Bmatrix} \tag{51}$$

The unit outward normal $\underset{\sim}{N}$ to the face i-j makes an angle θ to the r-axis and its components are given by $\{N\}^T = \langle\cos\theta \; 0 \; \sin\theta\rangle$. The conservation of mass requires that $\rho_0/\rho = \det [^1F]$, and finally, defining β to be the differential length along the face and hence the differential surface element to be $dA = 2\pi \, r \, \beta \, d\xi$, one obtains the expression for equivalent nodal loads as

$$\underset{4x1}{\{^2R\}} = -2\pi \int_{-1}^{1} \underset{4x3}{[\bar{\psi}]^T} \; \underset{3x3}{[^1F^{-1}]^T} \; \underset{3x1}{\{N\}} \; \underset{1x2}{\langle\psi\rangle} \; \underset{2x1}{\{^2p\}} \; r \, \beta \det [^1F] \, d\xi \tag{52}$$

3.7 Static Condensation Method

The incremental equations of motion, Eq. (11), can now be written at the element level as

$$\underset{8x8}{[M]} \; \underset{8x1}{\{\ddot{u}\}} + \underset{8x8}{[C_D]} \; \underset{8x1}{\{\dot{u}\}} + \underset{12x12}{[K_t]} \underset{12x1}{\{\hat{u}\}} = \underset{8x1}{\{^2R\}} - \underset{8x8}{[M]} \; \underset{8x1}{\{^1\ddot{u}\}} - \underset{8x8}{[C_D]} \; \underset{8x1}{\{^1\dot{u}\}} - \underset{12x1}{\{^1\hat{F}^R\}} \tag{53}$$

where $[K_t] = [K_o] + [K_G]$ is the element tangent stiffness matrix at time t. The equations corresponding to the incompatible modes are eliminated by the use of static condensation technique before assembly into the system of equations for the complete structure. This has the advantage that the total number of equations as well as the overall bandwidth of the structure are reduced. The method of condensing unwanted degrees of freedom is now well known [12] and proceeds as follows--

The stiffness matrix $[K_t]$, displacement vector $\{\hat{u}\}$ and nodal resisting forces $\{{}^1\hat{F}^R\}$ can be partitioned as

$$[K_t]_{12x12} = \left[\begin{array}{c|c} K_{uu} & K_{u\alpha} \\ \hline K_{\alpha u} & K_{\alpha\alpha} \end{array}\right]_{\substack{8x8 \quad 8x4 \\ 4x8 \quad 4x4}} ; \quad \{\hat{u}\}_{12x1} = \left\{\begin{array}{c} u \\ \hline \alpha \end{array}\right\}_{\substack{8x1 \\ 4x1}} ; \quad \{{}^1\hat{F}^R\} = \left\{\begin{array}{c} {}^1F^R \\ \hline {}^1F^R_\alpha \end{array}\right\}_{\substack{8x1 \\ 4x1}} \tag{54}$$

This enables the last four equations of (53) to be solved for $\{\alpha\}$, i.e.

$$\underset{4x1}{\{\alpha\}} = \underset{4x4}{[K_{\alpha\alpha}]^{-1}} \left(-\underset{4x8}{[K_{\alpha u}]} \underset{8x1}{\{u\}} - \underset{4x1}{\{{}^1F^R_\alpha\}}\right) \tag{55}$$

When this expression for $\{\alpha\}$ is substituted into the first eight equations of (53), one obtains the effective element stiffness matrix $[\bar{K}_t]$ and the effective nodal resisting forces $\{{}^1\bar{F}^R\}$ as

$$\underset{8x8}{[\bar{K}_t]} = \underset{8x8}{[K_{uu}]} - \underset{8x4}{[K_{u\alpha}]} \underset{4x4}{[K_{\alpha\alpha}]^{-1}} \underset{4x8}{[K_{\alpha u}]} \tag{56}$$

and

$$\underset{8x1}{\{{}^1\bar{F}^R\}} = \underset{8x1}{\{{}^1F^R\}} - \underset{8x4}{[K_{u\alpha}]} \underset{4x4}{[K_{\alpha\alpha}]^{-1}} \underset{4x1}{\{{}^1F^R_\alpha\}} \tag{57}$$

Eq. (53) is then reduced to the form

$$[M]\{\ddot{u}\} + [C_D]\{\dot{u}\} + [\bar{K}_t]\{u\} = \{^2R\} - [M]\{^1\ddot{u}\} - [C_D]\{^1\dot{u}\} - \{^1\bar{F}^R\} \quad (58)$$

Following the standard direct stiffness formulation, these element equations can then be directly assembled to form the incremental equations of motion for the structural system.

3.8 Solution of Equations

Step-by-step or direct integration procedures offer the only feasible method of solution for problems involving material and/or geometric nonlinearities. The method of Newmark [14] and Wilson, Farhoomand [15,16] have both been incorporated in the computer program developed during this study. The formulas needed for the implementation of these algorithms were summarized in earlier reports [2,4]. The inertia and damping forces are neglected in the case of quasi-static problems and Eq. (58) is solved repetitively using the Gaussian elimination technique. A modified incremental solution with equilibrium correction at each step is thus obtained and is the equivalent of a one-step Newton iteration scheme.

4. NUMERICAL EXAMPLES

Several numerical examples are presented in this section to demonstrate the capabilities of the developed computer program NEPAX (Nonlinear Elastic-Plastic analysis of AXisymmetric solids) for static and dynamic analysis of plane stress and axisymmetric problems. Comparisons are made with available analytical solutions as well as results of other known numerical analyses.

4.1 Elastic-Plastic Static Analysis of a S.S. Beam

The simply supported beam shown in Fig. 2 is of length L, thickness h and unit width. The material is assumed to be elastic-perfectly plastic and the behavior of the beam is studied when it is subjected to a uniformly distributed static load. Taking advantage of the symmetry about midspan and the antisymmetry about the neutral axis (using small displacement assumptions), only one quarter of the beam need be studied and is discretized by eight equal elements. Each element has two Gaussian integration points along the length and five Simpson integration points across the depth (i.e. a 2 x 5 integration scheme). The normalized load-displacement curve obtained using twenty load increments is presented in Fig. 2 and compares very well with the theoretical elastic-plastic solution of Prager and Hodge [17].

4.2 Elastic-Plastic Static Analysis of a Thick-Walled Cylinder

An infinitely long thick-walled cylinder shown as an insert in Fig. 3 is subjected to uniform internal pressure p_i. The cylinder has an inner radius of 1" and outer radius of 2" and is assumed to be made of elastic-perfectly plastic material with the following properties:

Young's modulus, $E = 8.67 \times 10^6$ psi

Poisson's ratio, $\nu = 0.3$

Yield stress, $\sigma_y = 1732$ psi

The purpose of this analysis is to compare the finite element results with the analytical elastic-plastic solutions presented by Hodge and White [18].

The cylinder is discretized by ten equal elements (2 x 2 integration scheme) in the radial direction and analyzed using fifteen load increments reaching a total internal pressure of 1400 psi. Fig. 3 displays the radial displacement at the outer face of the cylinder as a function of increasing internal pressure while Fig. 4 shows the radial, circumferential and axial stress distributions across the cylinder thickness at an internal pressure of 1250 psi with the elastic-plastic boundary being located at $r/a = 1.5$. The agreement between the finite element results and the analytical solution [18] is excellent as may be seen from Figs. 3 and 4 and further demonstrates the capability of the program to analyze elastic-plastic problems with a high degree of accuracy.

4.3 Large Displacement Static Analysis of a Spherical Cap

The static analysis of an elastic spherical cap under a concentrated apex load has been studied by several authors - among them Mescall [19], Stricklin [20] and Bathe *et al* [21] - as the high degree of nonlinearity exhibited by this structure poses quite a severe test for any large displacement formulation. This cap is shown as an insert in Fig. 5 and has the following dimensions:

Radius of curvature,	R	= 4.76 in.
Shell thickness,	h	= 0.01576 in.
Rise of the shell,	H	= 0.0859 in.
Half angle of opening,	α	= 10.9°

The material is assumed to be isotropic, linear elastic with Young's modulus $E = 10 \times 10^6$ psi and Poisson's ratio $\nu = 0.3$. The purpose of this analysis is to compare the finite element results with the known numerical solutions and to demonstrate the capabilities of the present program to treat large

displacement problems.

The cap is discretized by ten equal elements (2 x 2 integration scheme) from the apex to the support. The normalized apex displacement is shown in Fig. 5 as a function of the applied load for three different loading schemes. The solutions of Stricklin [20] and Bathe et al [21] (both employing 100 equal load steps) are also plotted in the same figure.

The result of using twenty equal steps of 5 lbs. is that the solution drifts away considerly in the softening region. But once the cap folds over and begins to stiffen, the results follow the solution of [21] even with this coarse scheme of loading. Using fifty equal increments of 2 lbs. improves the solution considerably as may be seen from Fig. 5. Since the behavior of the cap is almost linear once it enters the stiffening phase, it is obvious that fine load increments are needed only to capture the softening behavior correctly, after which coarser load steps could be taken without any loss of accuracy. Hence, a final loading scheme consisting of fifty equal steps of 1 lb., followed by five steps of 2 lbs. and finally eight steps of 5 lbs. (thus 63 steps over a total of 100 lbs.) is employed and gives a solution which is identical to that of [21]. The load-displacement curve of [20] is slightly different from the current solution and could be attributed to the formulation employed by Stricklin [20] which considers the nonlinearities as giving rise to additional effective loads rather than making a contribution to the structural stiffness.

4.4 Large Displacement Static and Dynamic Analysis of a Cantilever

The large displacement analysis of an elastic cantilever shown as an insert in Fig. 6 is taken up as the next example. An analytical solution has been presented by Holden [22] for the static analysis of a cantilever under a uniformly distributed load and shows the stiffening

behavior of the beam with increasing displacements. It should be noted, however, that the loading in [22] is assumed to be conservative (the direction of load application remains fixed in space) with the result that, as the displacements increase, a significant part of the loading is sustained by membrane rather than flexural action. If, on the other hand, a nonconservative load of the pressure type is considered, the load remains normal to the beam at all times and must, therefore, be sustained primarily by flexure. This would result in the stiffening of the cantilever to be much less than that predicted by Holden. Indeed, in the case of dynamic loading, such as due to a blast, it is more realistic to assume a pressure type loading. Hence the correct identification of the applied load is of primary importance in a large displacement analysis and the behavior of the cantilever is studied here under the action of both the gravity type conservative load and nonconservative pressure load.

The material of the cantilever is assumed to be isotropic, linear elastic and the pertinent dimensions as well as material properties are as follows:

Length, $L = 10$ in.

Depth, $h = 1$ in.

Width, $b = 1$ in.

Young's modulus, $E = 1.2 \times 10^{4}$ psi

Poisson's ratio, $\nu = 0.2$

Mass density, $\rho = 1.0 \times 10^{-6}$ lb.-sec^{2}./in^{4}.

The cantilever is discretized by five equal elements (2 x 2 integration scheme) and a static load of 10 lbs./in. is applied using 100 equal increments. The normalized load-displacement results are presented in Fig. 6. The agreement with the analytical solution [22] is excellent for the case of gravity type conservative loading. In addition, it may also be observed

that the stiffening of the cantilever is considerably less under the influence of nonconservative pressure type loading which is to be expected in view of the discussion in the preceding paragraph.

The dynamic analysis of this cantilever under a gravity type uniform step load of 2.85 lb./in. has been presented by Bathe et al [21]. The displacement-time results obtained in the present study using Newmark integration method (with $\gamma = 0.5$ and $\beta = 0.25$) are plotted in Fig. 7 and compare very well with those of [21]. The nonlinear response has a significantly smaller amplitude and effective period of vibration compared to the linear solution. In addition, the linear and nonlinear static displacements (obtained from Fig. 6) for a 2.85 lb./in. gravity type load are also indicated in Fig. 7 and approximate the mean displacements around which the cantilever vibrates in the corresponding dynamic analyses.

The large displacement dynamic analysis is also carried out for a 2.85 lb./in. uniform step pressure and Fig. 8 shows the displacement-time histories for both types of loading as well as the results of the linear analysis. The three corresponding static solutions (from Fig. 6) are also indicated in this figure. The peak amplitudes and period of vibration of the beam under the pressure load are smaller than the results of the linear analysis but greater than the values obtained from the nonlinear analysis using the gravity type conservative load. These results are consistent with the observations made earlier in the case of static analysis and once again emphasize the importance of defining the applied load correctly.

4.5 Dynamic Response of a Shallow Spherical Cap

A shallow spherical cap subjected to a uniformly distributed step pressure is selected as the last example. The geometry, material properties and load-time history are given in Fig. 9. Ten equal elements (2 x 2 integration scheme for elastic analysis and 2 x 5 integration for

elastic-plastic analysis) are employed to discretize the shell from the apex to the support. The time integration is carried out using the Newmark method (with $\gamma = 0.5$ and $\beta = 0.25$) with 10×10^{-6} sec. time steps.

Uniform external step pressure of 600 psi is applied on the cap and the dynamic response obtained for linear elastic as well as linear and nonlinear elastic-plastic cases. The apex displacement of the cap is plotted in Fig. 10 for all three cases as a function of time. The effect of the nonlinearities on the dynamic response of this cap is significant although the behavior of this cap is not highly nonlinear when the intensity of loading considered here is applied in a quasi-static manner. The motion of the cap is damped by the unrecoverable mechanical work expended in plastic deformation with the result that the peak amplitudes are reduced and the periods of vibration increased as compared to the elastic solution. In addition, it should be noted that the mean displacement around which the cap vibrates is greater in the elastic-plastic cases compared to the elastic response wherein the vibration takes place around the static displacement.

The geometrically linear elastic and elastic-plastic solutions are compared in Fig. 11 with the solutions obtained in [2] using the ten node isoparametric elements. The agreement is good in the case of the elastic analyses, the slight differences in the peak amplitude being attributable to the different structural discretizations employed. The elastic-plastic solutions differ to a greater extent and it should be noted in this connection that the boundary conditions at the fixed end are idealized differently in the two analyses. The pinching effect at the support has been avoided in [2] by allowing two of the three nodal points to slide along the inclined support. It is shown in [2] that an alternate boundary condition wherein such sliding is not permitted affects the

effective stress distribution (upon which the yield condition is based) and leads to an increase of about 10% in the peak amplitude of the cap under 445 psi step pressure. The differences between the two elastic-plastic solutions in Fig. 11 can then be attributed to a large extent to the fact that the latter boundary condition has been employed in the present study as the current program is capable of specifying the boundary conditions only along the global r- and z-axes. For completely enclosed spaces, such as occur in pressure vessels, this problem does not arise.

The elastic-plastic (linear and nonlinear geometry) responses are finally compared in Fig. 12 with the responses obtained in [4] using degenerate isoparametric shell elements. Although the two sets of solutions exhibit the same trend as far as vibration periods and phase shifts are concerned, the peak amplitudes do not agree very well. However, such a comparison is complicated due to several factors that need to be taken into consideration. Whereas a two dimensional solid element is employed in the present study, the one used in [4] is a degenerate shell element in which transverse normal stresses are assumed to be negligible and do not enter into the computation of effective stresses which control the plastic behavior. In addition, as discussed earlier with reference to Fig. 11, the boundary conditions used also affect the effective stresses. Also, no artificial damping is involved in the numerical time integration in this investigation whereas the δ-control is used in the Newmark method ($\delta = 0.05$, $\gamma = 0.55$ and $\beta = 0.276$) in the solutions obtained in [4] and introduces some damping of the peaks. It is of interest to note that this cap has also been studied by Bathe et al [21] whose results (not plotted in the figure), using an eight nodal point isoparameteric element, give peak amplitudes

that lie in between those of [4] and this study. Thus no conclusions can be readily drawn regarding the accuracy of the various numerical solutions in the absence of some parametric studies to determine their convergence or experimental results with which comparisons could be made.

5. CONCLUSIONS

An efficient computer program for elastic-plastic, large displacement static and dynamic analysis of axisymmetric solids has been developed using quadrilateral elements with incompatible modes. The discretized incremental finite element equations, obtained using a general Lagrangian formulation, are solved by step-by-step numerical time integration schemes with equilibrium correction at each step. The flow theory of plasticity with von Mises yield criterion is used in the plastic range. The sample problems considered have all been solved using the isotropic hardening rule or assuming elastic-perfectly plastic behavior although the linear kinematic hardening law is also incorporated as an option in the computer program. Several sets of material properties may be defined and the behavior of different elements in a structure may then be governed by different material laws, thus enabling the study of composite systems.

The addition of incompatible modes in a quadrilateral element greatly improves its accuracy. However, these elements should not be badly distorted in shape and this may impose some restrictions in passing from a single layered to multilayered mesh or in changing the number of layers in a continuous mesh. In this connection, it may be advantageous to include options in the program for isoparametric elements with more than four nodes. Further, in many applications, the parts of the structure which behave primarily as shells could be represented advantageously by the degenerate isoparametric shell element if an option were also provided for such an element.

The merits of the different elements in terms of computational efficiency are rather difficult to judge from the samll-scale problems such as those studied here. But the general observation can be made

that, on a per element basis, the quadrilateral element used in the present study is competitive with the degenerate shell element and considerable more efficient than the ten node isoparameteric element. However, the number of elements required to achieve a comparable level of accuracy in the discretization using the different elements is really problem dependent. Hence, the proper selection of elements and mesh lay-out for a given problem must be based on available information such as the geometry of the structure, type of loading and possible some knowledge of the stress gradients.

ACKNOWLEDGEMENTS

The authors take this opportunity to thank Mr. George Demitrack, Chief, Engineering Research Branch, Picatinny Arsenal, for the continuing interest displayed in the progress of this work. The assistance of graduate student Mr. M. Galuzzi with the examples is also appreciated. The computer time and facilities were provided by the Computer Center, University of California, Berkeley.

REFERENCES

1. Larsen, P.K. and Popov, E. P., "Elastic-Plastic Analysis of Axisymmetric Solids Using Isoparametric Finite Elements," SESM Report 71-2, Depart. of Civil Eng., University of California, Berkeley, 1971.

2. Nagarajan, S. and Popov, E.P., "Elastic-Plastic Dynamic Analysis of Axisymmetric Solids," SESM Report 73-9, Depart. of Civil Eng., University of California, Berkeley, 1973.

3. Larsen, P.K., "Large Displacement Analysis of Shells of Revolution Including Creep, Plasticity and Viscoelasticity," Ph.D. dissertation, SESM Report 71-22, Depart. of Civil Eng., University of California, Berkeley, 1971.

4. Nagarajan, S., "Nonlinear Static and Dynamic Analysis of Shells of Revolution Under Axisymmetric Loading," Ph.D. dissertation, SESM Report 73-11, Depart. of Civil Eng., University of California, Berkeley, 1973.

5. Oden, J.T., Finite Elements of Nonlinear Continua, McGraw-Hill, 1972.

6. Larsen, P.K. and Popov, E.P., "Large Displacement Analysis of Viscoelastic Shells of Revolution," Computer Methods in Applied Mech. and Eng., v. 3, pp. 237-253, 1974.

7. Khojasteh-Bakht, M., "Analysis of Elastic-Plastic Shells of Revolution Under Axisymmetric Loading by the Finite Element Method," Ph.D. dissertation, SESM Report 67-8, Depart. of Civil Eng., University of California, Berkeley, 1967.

8. Prager, W., "The Theory of Plasticity: A Survey of Recent Achievements," (James Clayton Lecture) Proc. Inst. Mech. Eng., v. 169, No. 21, pp. 41-52, 1955.

9. Ziegler, H., "A Modification of Prager's Hardening Rule," Quart. Appl. Math, v. 17, pp. 55-65, 1959.

10. Ergatoudis, J., Irons, B.M. and Zienkiewicz, O.C.,"Curved, Isoparametric, 'Quadrilateral' Elements for Finite Element Analysis," Int. J. of Solids and Structures, v. 4, pp. 31-42, 1968.

11. Ahmad, S., Irons, B.M. and Zienkiewicz, O.C., "Curved Thick Shell and Membrane Elements wtih Particular Reference to Axisymmetric Problems," Proc. 2nd Conf. on Matrix Methods in Struct. Mech., AFFDL-TR-68-150, 1968.

12. Wilson, E.L., "Solid SAP, A Static Analysis Program for Three-Dimensional Solid Structures," SESM Report 71-19, Depart. of Civil Eng., University of California, Berkelely, 1971 (revised March 1972).

13. Abramowitz, M. and Stegun, I.A., Handbook of Mathematical Functions, National Bureau of Standards, 1964.

14. Newmark, N.M., "A Method of Computation for Structural Dynamics," Proc. ASCE, v. 85, EM3, pp. 67-94, 1959.

15. Farhoomand, I., "Nonlinear Dynamic Stress Analysis of Two-Dimensional Solids," Ph.D. dissertation, Depart. of Civil Eng., University of California, Berkeley, 1970.

16. Wilson, E.L., Farhoomand, I. and Bathe, K.J., "Nonlinear Dynamic Analysis of Complex Structures," Int. J. of Earthquake Eng. and Struct. Dynamics, v. 1, pp. 241-252, 1973.

17. Prager, W. and Hodge, P.G., Theory of Perfectly Plastic Solids, Dover, 1968.

18. Hodge, P.G. and White, G.H., "A Quantitative Comparison of Flow and Deformation Theories of Plasticity," J. Appl. Mech., v. 17, pp. 180-184, 1950.

19. Mescall, J.F., "Large Deflections of Spherical Shells Under Concentrated Loads," J. Appl. Mech., v. 32, pp. 936-938, 1965.

20. Stricklin, J.A., "Geometrically Nonlinear Static and Dynamic Analysis of Shells of Revolution," High Speed Computing of Elastic Structures, Proc. of the Symposium of IUTAM, University of Liege, pp. 383-411, 1970.

21. Bathe, K.J., Ozdemir, H. and Wilson, E.L., "Static and Dynamic Geometric and Material Nonlinear Analysis," SESM Report 74-4, Depart. of Civil Eng., University of California, Berkeley, 1974.

22. Holden, J.T., "On the Finite Deflections of Thin Beams," Int. J. of Solids and Structures, v. 8, pp. 1051-1055, 1972.

APPENDIX A. DISPLACEMENT GRADIENT MATRIX

This appendix outlines the procedure used to evaluate the displacement gradient matrix [B] in Eqs. (35,36) which relates the displacement gradients $\{u_\partial\}$ and $\{{}^1u_\partial\}$ to the displacements $\{\hat{u}\}$ and $\{{}^1\hat{u}\}$ in the quadrilateral element with incompatible modes.

The geometry and displacement fields are given by

$$\begin{Bmatrix} r \\ z \end{Bmatrix} = \sum_{i=1}^{4} \phi_i (\xi,\eta) \begin{Bmatrix} r_i \\ z_i \end{Bmatrix} \tag{21}$$

and

$$\begin{Bmatrix} u \\ w \end{Bmatrix} = \sum_{i=1}^{4} \phi_i (\xi,\eta) \begin{Bmatrix} u_i \\ w_i \end{Bmatrix} + \phi_5 (\xi,\eta) \begin{Bmatrix} \alpha_1 \\ \alpha_2 \end{Bmatrix} + \phi_6(\xi,\eta) \begin{Bmatrix} \alpha_3 \\ \alpha_4 \end{Bmatrix} \tag{25}$$

The chain rule of differentiation gives

$$\begin{Bmatrix} \partial/\partial r \\ \partial/\partial z \end{Bmatrix} = \frac{1}{\det J} [J] \begin{Bmatrix} \partial/\partial \xi \\ \partial/\partial \eta \end{Bmatrix} \tag{A.1}$$

where [J] is the Jacobian matrix given by

$$[J] = \begin{bmatrix} \partial z/\partial \eta & -\partial z/\partial \xi \\ -\partial r/\partial \eta & \partial r/\partial \xi \end{bmatrix} \tag{A.2}$$

and

$$|J| = \det J = \frac{\partial z}{\partial \eta} \frac{\partial r}{\partial \xi} - \frac{\partial z}{\partial \xi} \frac{\partial r}{\partial \eta} \tag{A.3}$$

Combining Eqs. (21) and (A.3), one gets

$$|J| = \phi_{i,\xi}\, r_i\, \phi_{j,\eta}\, z_j - \phi_{i,\eta}\, r_i\, \phi_{j,\xi}\, z_j$$

or

$$|J| = r_i \left(\phi_{i,\xi}\, \phi_{j,\eta} - \phi_{i,\eta}\, \phi_{j,\xi}\right) z_j \tag{A.4}$$

Let

$$[P] = \phi_{i,\xi}\, \phi_{j,\eta} - \phi_{i,\eta}\, \phi_{j,\xi} \tag{A.5}$$

Then

$$|J| = \langle r \rangle [P] \{z\} \tag{A.6}$$

where $\langle r \rangle = \{r\}^T$ and $\{z\}$ are vectors of nodal point global coordinates.

The global displacement gradients can be derived in a similar manner using Eqs. (21,25) and the chain rule of differentiation, Eqs. (A.1, A.2), e.g.

$$\frac{\partial u}{\partial r} = \frac{1}{|J|}\left(\frac{\partial u}{\partial \xi}\frac{\partial z}{\partial \eta} - \frac{\partial u}{\partial \eta}\frac{\partial z}{\partial \xi}\right)$$

$$= \frac{1}{J}\left[\left(u_i \phi_{i,\xi} + \alpha_1 \phi_{5,\xi} + \alpha_3 \phi_{6,\xi}\right)\phi_{j,\eta} z_j - \left(u_i \phi_{i,\eta} + \alpha_1 \phi_{5,\eta} + \alpha_3 \phi_{6,\eta}\right)\phi_{j,\xi} z_i\right] \quad i,j=1,4$$

For convenience of notation, define the following:

$$[\bar{P}] = \left(\phi_{i,\xi}\phi_{j,\eta} - \phi_{i,\eta}\phi_{j,\xi}\right) \quad i=1,6; \quad j=1,4 \tag{A.7}$$

$$\langle U \rangle = \langle u\ \alpha_1\ \alpha_3 \rangle = \langle u_1\ u_2\ u_3\ u_4\ \alpha_1\ \alpha_3 \rangle \tag{A.8}$$

$$\langle W \rangle = \langle w\ \alpha_2\ \alpha_4 \rangle = \langle w_1\ w_2\ w_3\ w_4\ \alpha_2\ \alpha_4 \rangle \tag{A.9}$$

$$\{Y\} = \frac{1}{|J|}[\bar{P}]\{z\} \quad \text{and} \quad \{X\} = -\frac{1}{|J|}[\bar{P}]\{r\} \tag{A.10}$$

Then, $$\frac{\partial u}{\partial r} = \frac{1}{|J|}\langle U \rangle [\bar{P}]\{z\} = \langle U \rangle \{Y\} \tag{A.11}$$

In a similar manner, the expressions for the other displacement gradients $\frac{u}{r}$, $\frac{\partial u}{\partial z}$, $\frac{\partial w}{\partial r}$ and $\frac{\partial w}{\partial z}$ can also be obtained as

$$\frac{u}{r} = \frac{1}{r}\left(\phi_i u_i + \phi_5 \alpha_1 + \phi_6 \alpha_3\right) \quad i=1,4 \tag{A.12}$$

$$\frac{\partial u}{\partial z} = -\frac{1}{|J|}\langle U \rangle [\bar{P}]\{r\} = \{U\}\{X\} \tag{A.13}$$

$$\frac{\partial w}{\partial r} = \frac{1}{|J|}\langle W \rangle [\bar{P}]\{z\} = \langle W \rangle \{Y\} \tag{A.14}$$

and $$\frac{\partial w}{\partial z} = -\frac{1}{|J|}\langle W \rangle [\bar{P}]\{r\} = \langle W \rangle \{X\} \tag{A.15}$$

Finally, defining

$$\langle \hat{u} \rangle = \langle u_1 \; w_1 \; u_2 \; w_2 \; u_3 \; w_3 \; u_4 \; w_4 \; \alpha_1 \; \alpha_2 \; \alpha_3 \; \alpha_4 \rangle \tag{A.16}$$

the displacement gradient matrix [B] can be written as

$$[B] = \begin{bmatrix} Y_1 & 0 & Y_2 & 0 & Y_3 & 0 & Y_4 & 0 & Y_5 & 0 & Y_6 & 0 \\ \phi_1 & 0 & \phi_2 & 0 & \phi_3 & 0 & \phi_4 & 0 & \phi_5 & 0 & \phi_6 & 0 \\ X_1 & 0 & X_2 & 0 & X_3 & 0 & X_4 & 0 & X_5 & 0 & X_6 & 0 \\ 0 & Y_1 & 0 & Y_2 & 0 & Y_3 & 0 & Y_4 & 0 & Y_5 & 0 & Y_6 \\ 0 & X_1 & 0 & X_2 & 0 & X_3 & 0 & X_4 & 0 & X_5 & 0 & X_6 \end{bmatrix} \tag{A.17}$$

The last four columns of this 5 x 12 matrix operate on the incompatible displacement amplitudes and can be readily suppressed if desired in the computer program.

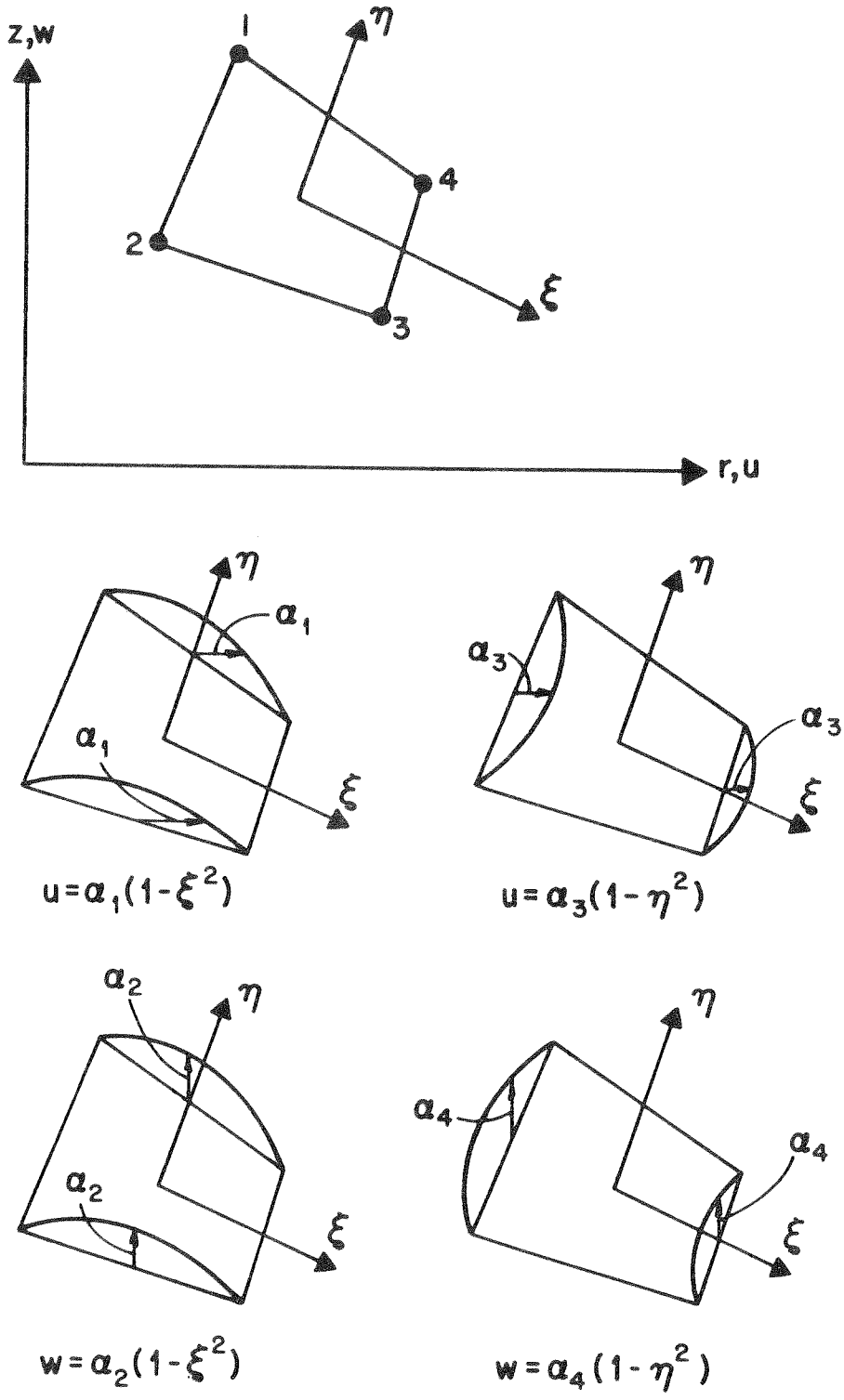

FIG. 1 QUADRILATERAL ELEMENT AND INCOMPATIBLE MODES

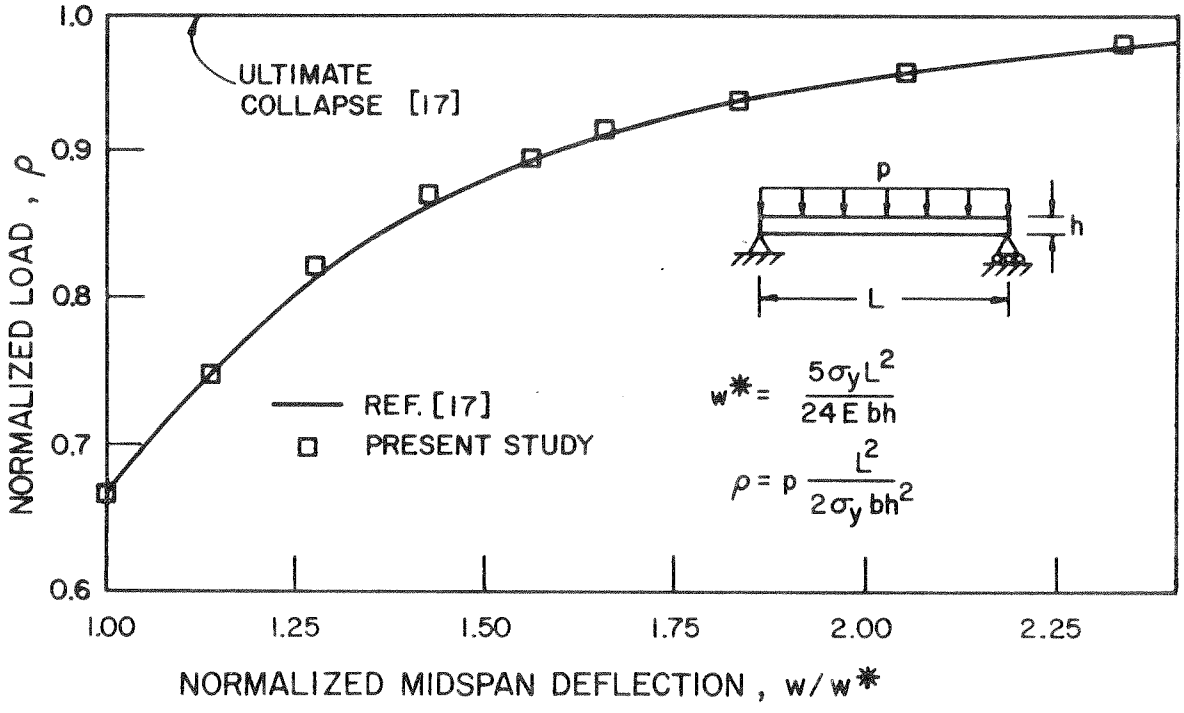

FIG. 2 ELASTIC-PLASTIC ANALYSIS OF A S.S. BEAM

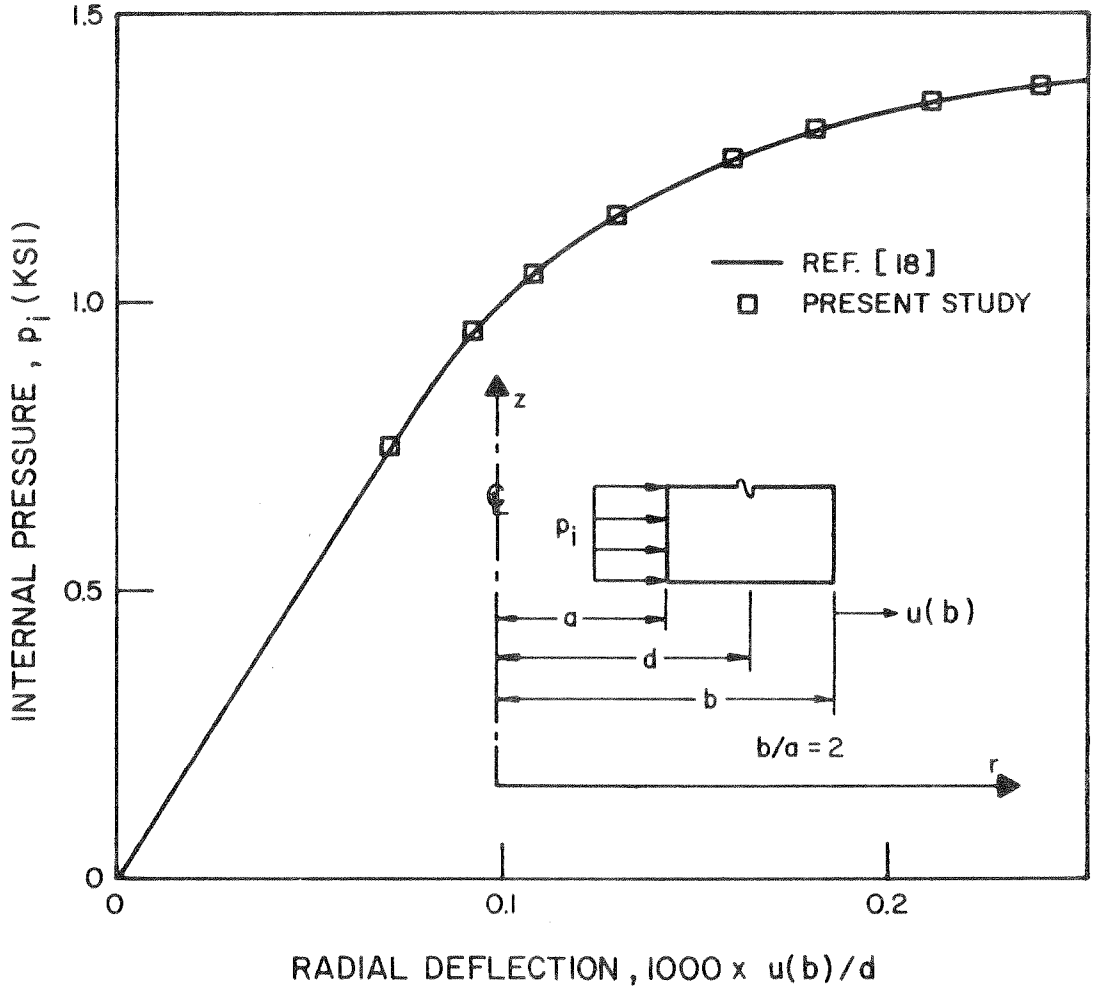

FIG. 3 ELASTIC-PLASTIC ANALYSIS OF A THICK-WALLED CYLINDER

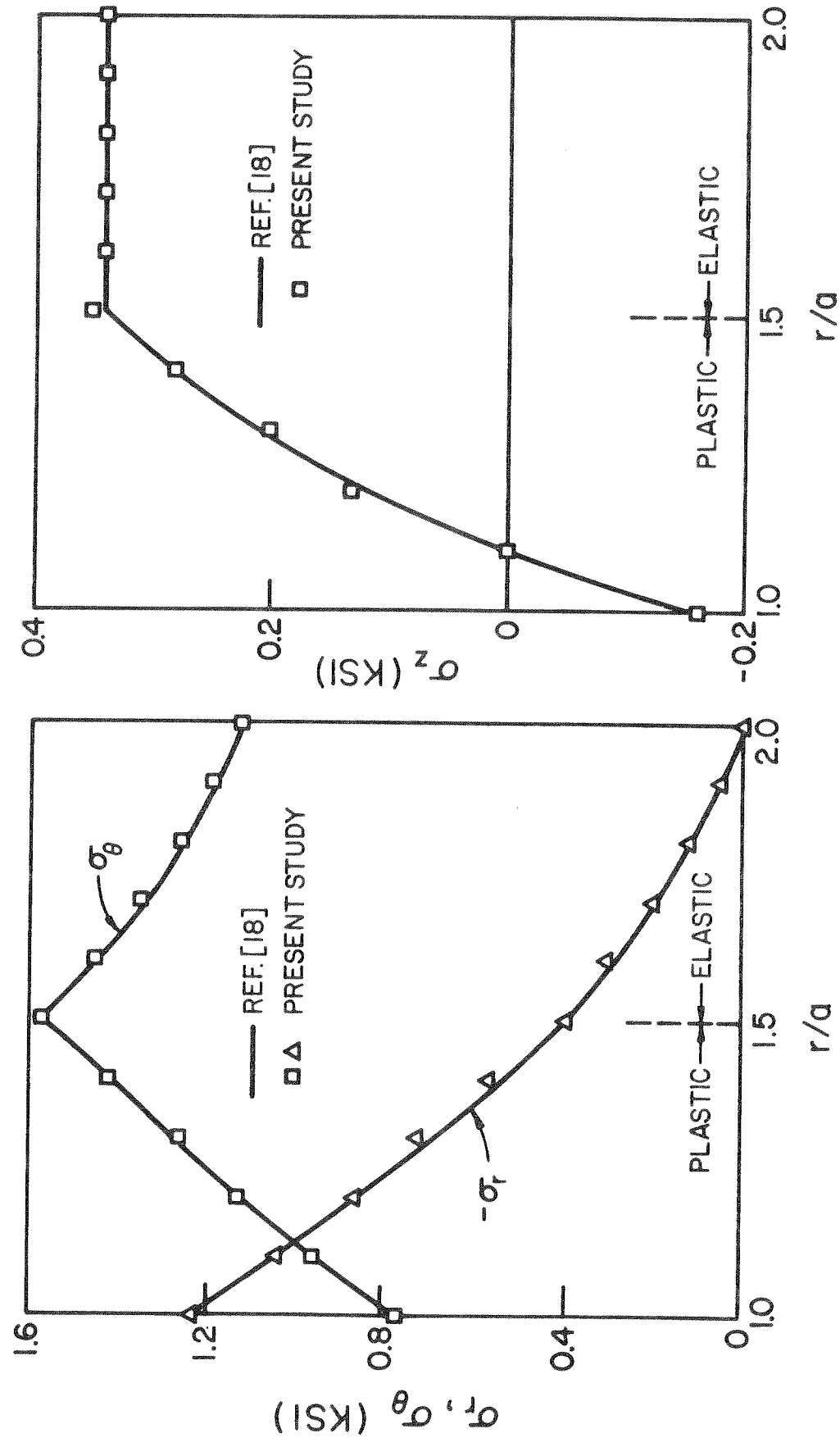

FIG. 4 STRESS DISTRIBUTIONS IN THICK-WALLED CYLINDER AT p_i=1250 PSI

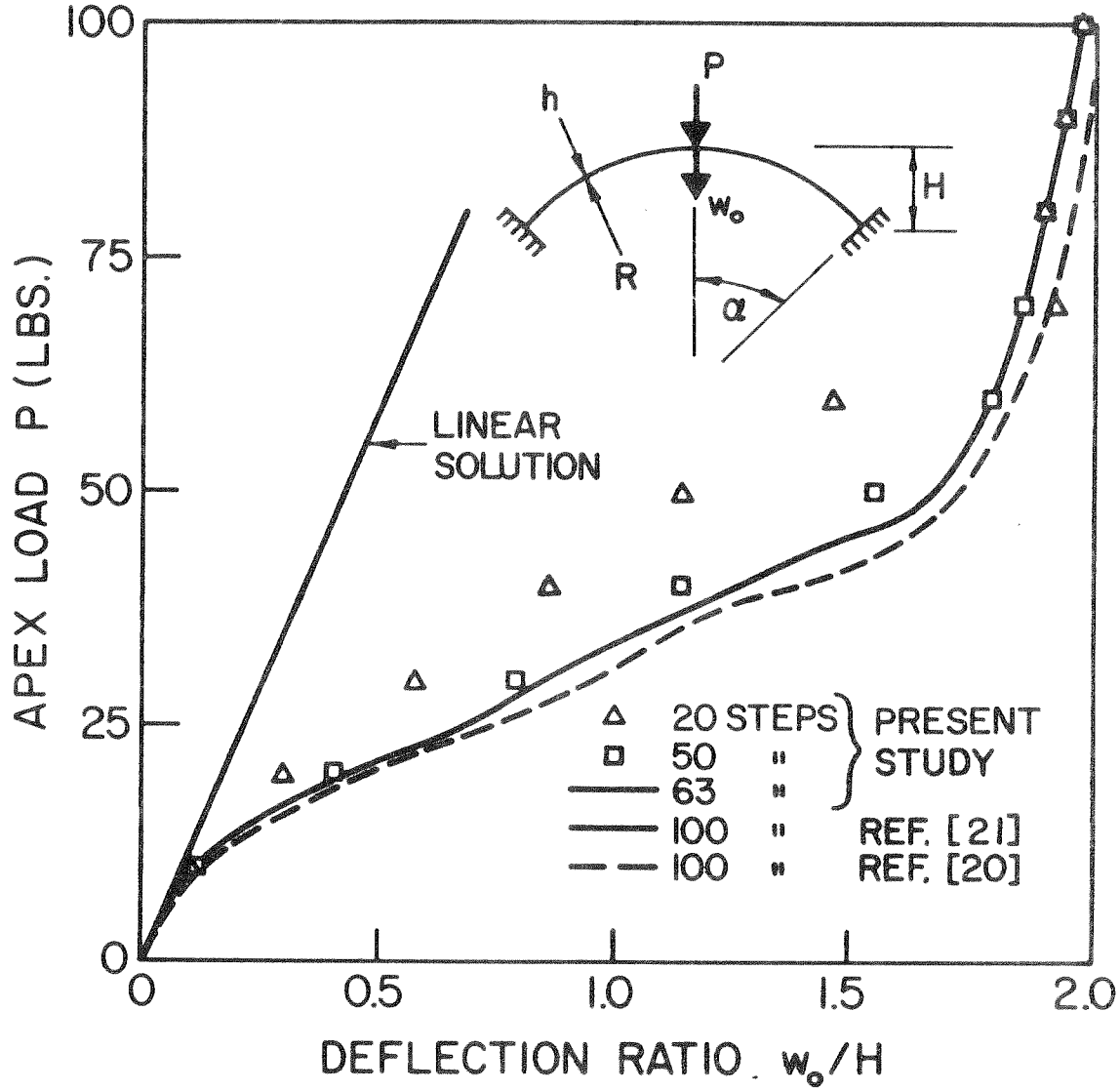

FIG. 5 LARGE DISPLACEMENT ANALYSIS OF SPHERICAL SHELL

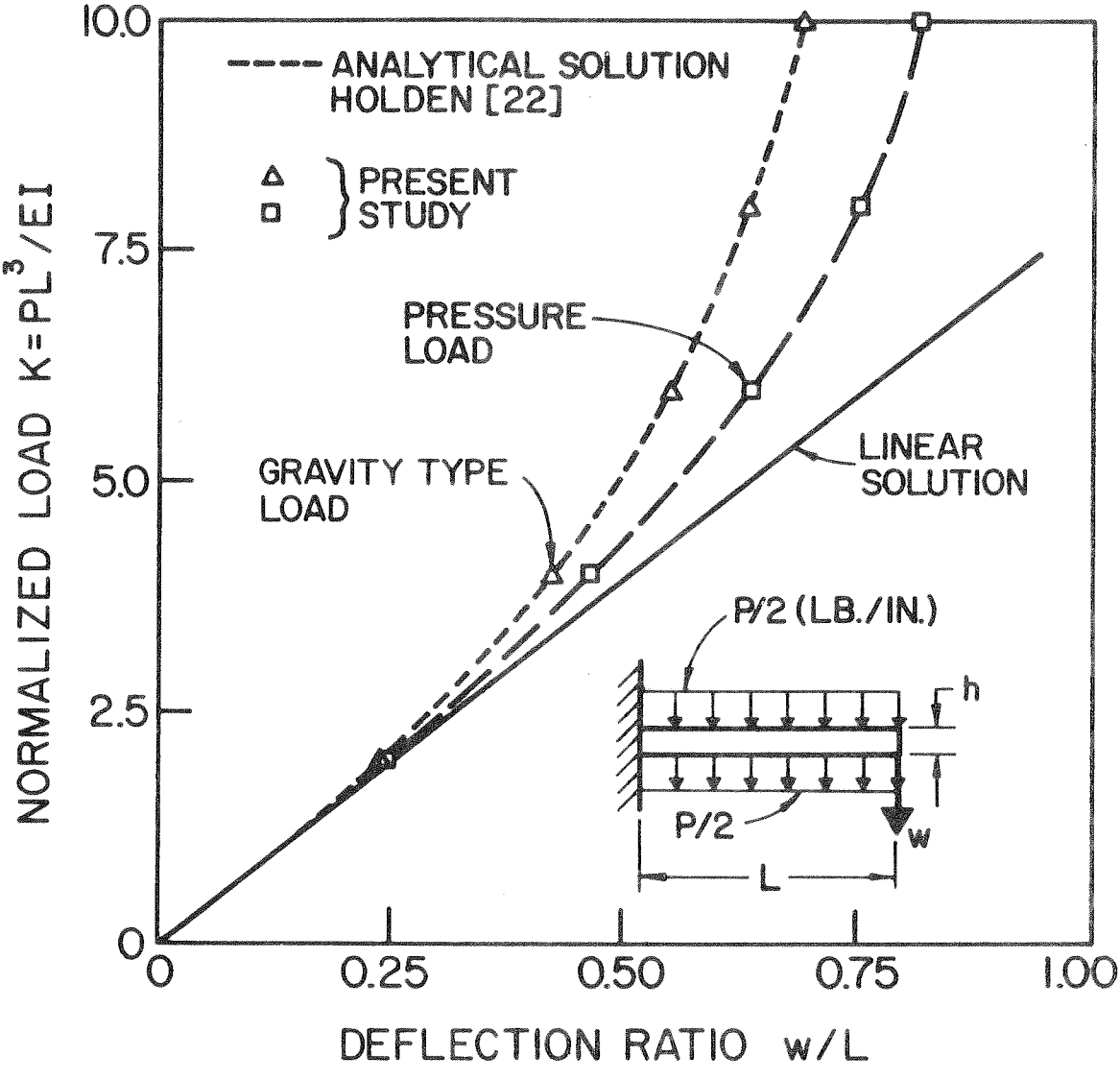

FIG. 6 LARGE DISPLACEMENT STATIC ANALYSIS OF ELASTIC CANTILEVER

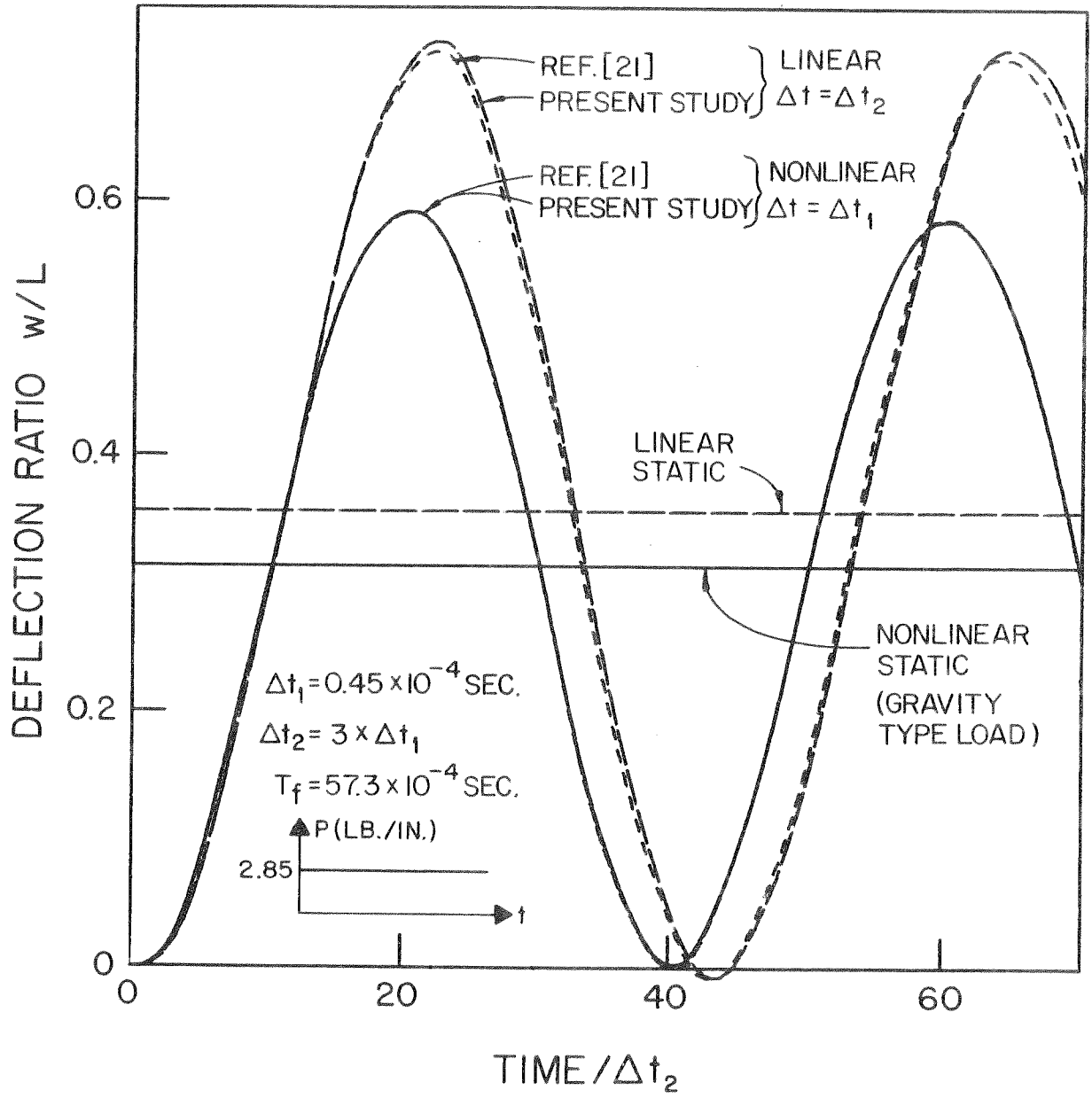

FIG. 7 DYNAMIC RESPONSE OF ELASTIC CANTILEVER

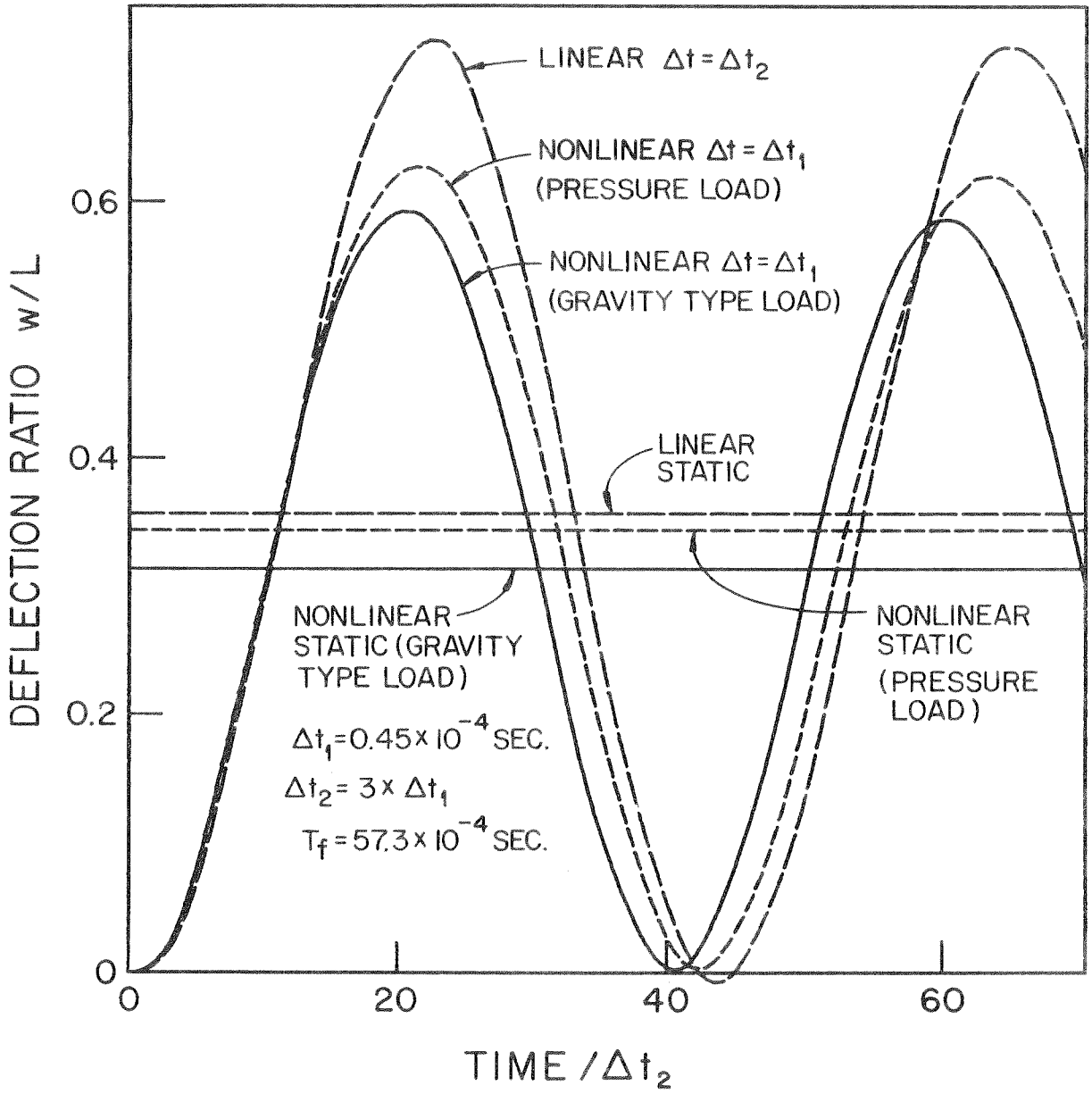

FIG. 8 DYNAMIC RESPONSE OF ELASTIC CANTILEVER FOR DIFFERENT LOADINGS

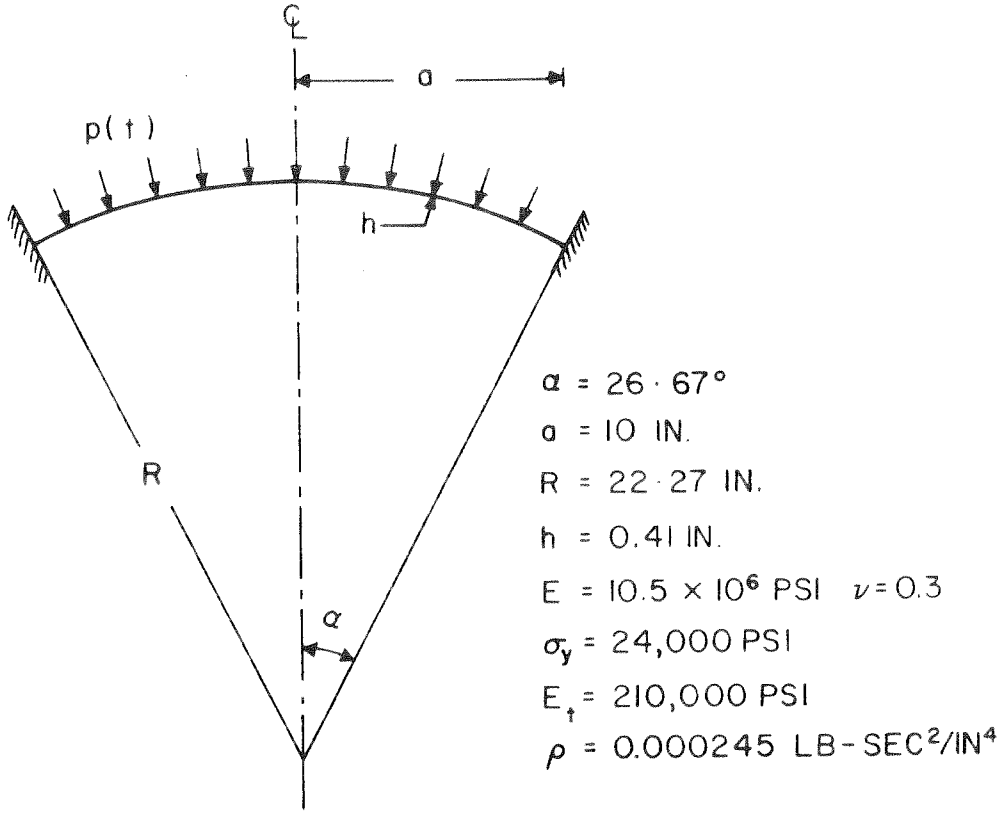

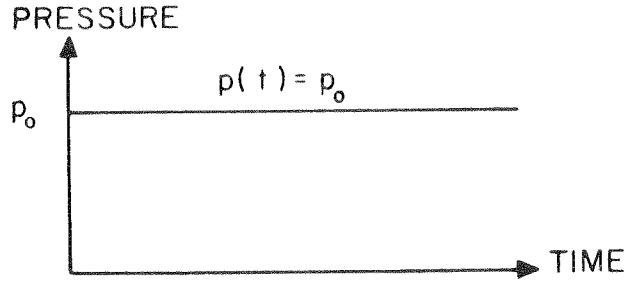

FIG. 9 SHALLOW SPHERICAL SHELL CAP AND PRESSURE-TIME HISTORY

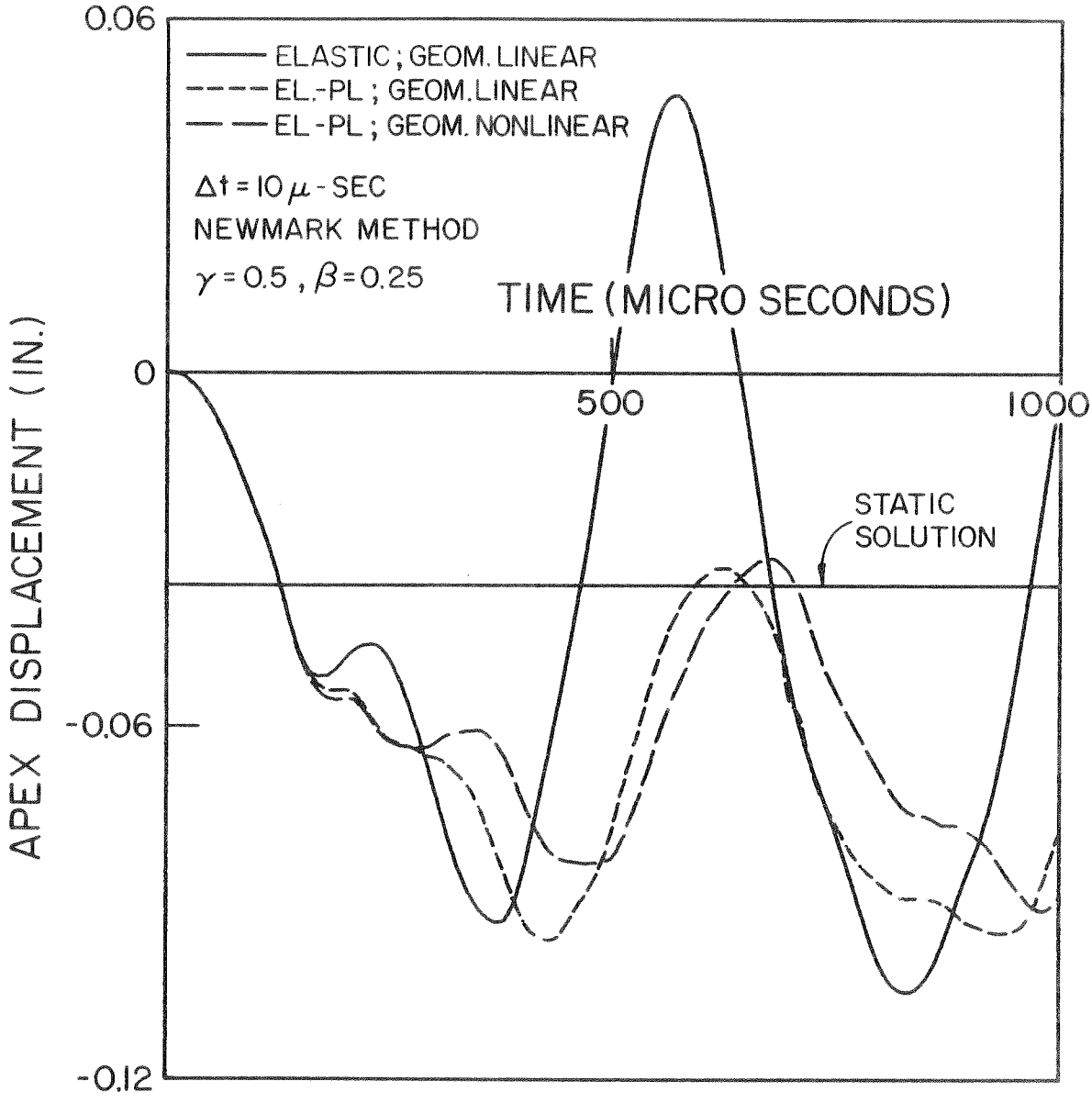

FIG. 10 DYNAMIC RESPONSE OF SPHERICAL CAP UNDER 600 PSI EXTERNAL STEP PRESSURE

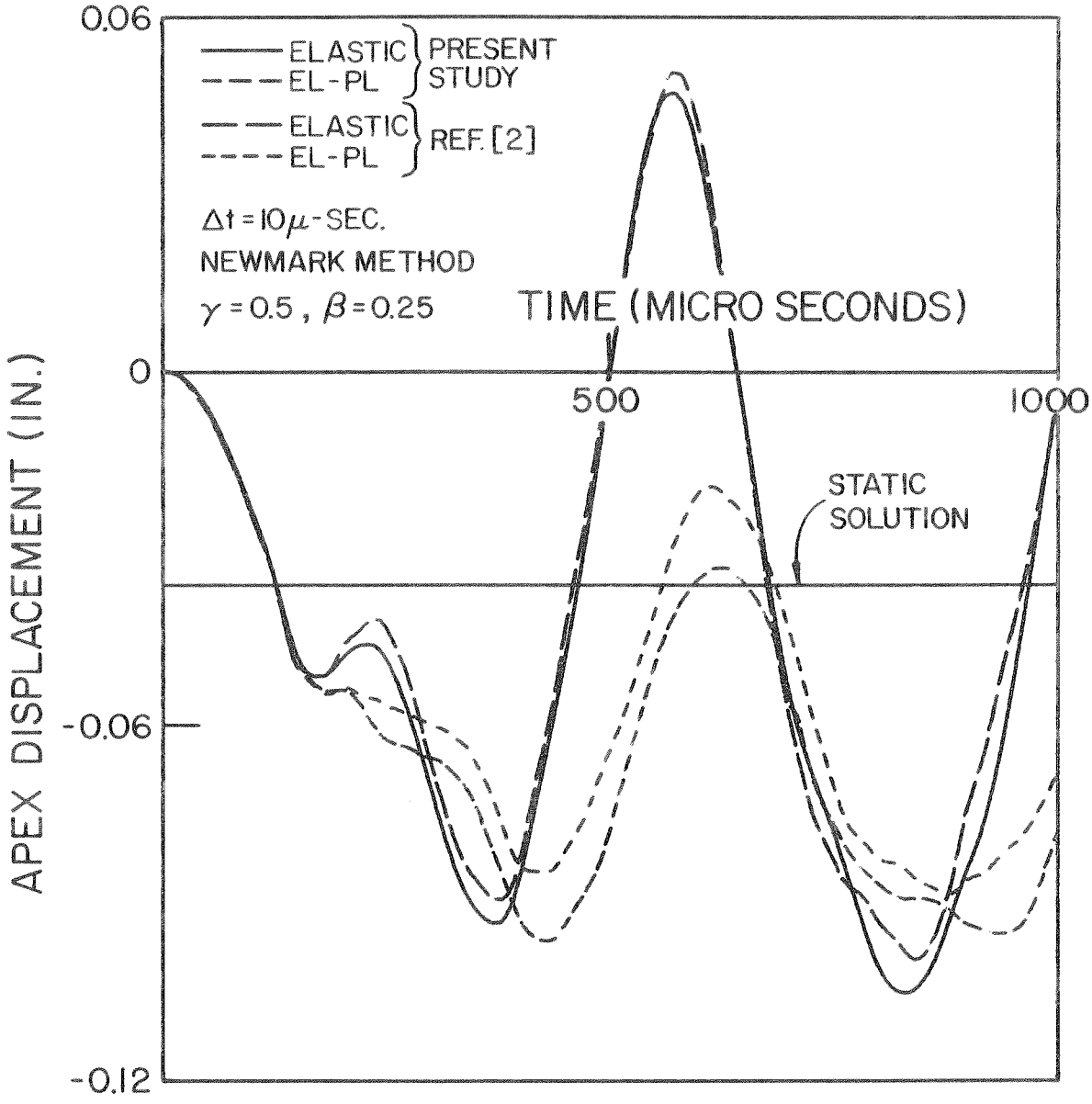

FIG. 11 GEOM. LINEAR DYNAMIC RESPONSE OF SPHERICAL CAP UNDER STEP PRESSURE

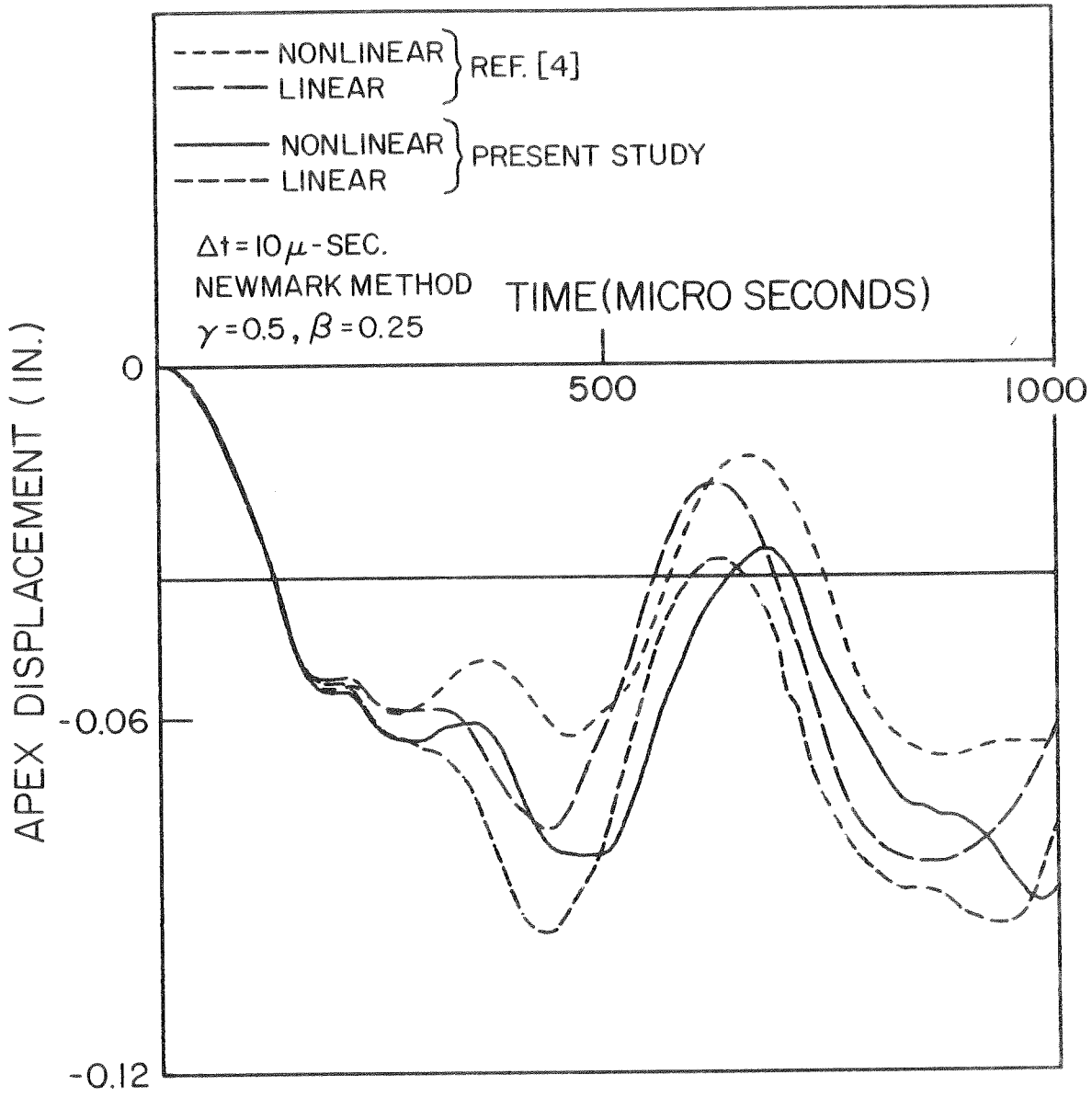

FIG. 12 DYNAMIC ELASTIC-PLASTIC RESPONSE OF SPHERICAL CAP UNDER STEP PRESSURE

UNCLASSIFIED

SECURITY CLASSIFICATION OF THIS PAGE *(When Data Entered)*

REPORT DOCUMENTATION PAGE		READ INSTRUCTIONS BEFORE COMPLETING FORM
1. REPORT NUMBER UC SESM 74-9	2. GOVT ACCESSION NO.	3. RECIPIENT'S CATALOG NUMBER
4. TITLE *(and Subtitle)* NONLINEAR FINITE ELEMENT DYNAMIC ANALYSIS OF AXISYMMETRIC SOLIDS		5. TYPE OF REPORT & PERIOD COVERED Interim: July '73-July '74 6. PERFORMING ORG. REPORT NUMBER UC SESM 74-9
7. AUTHOR(s) S. Nagarajan and E. P. Popov		8. CONTRACT OR GRANT NUMBER(s) DAAA21-72-C-0727
9. PERFORMING ORGANIZATION NAME AND ADDRESS Division of Structural Engrg. & Struct. Mechanics Department of Civil Engineering University of California, Berkeley, CA 94720		10. PROGRAM ELEMENT, PROJECT, TASK AREA & WORK UNIT NUMBERS
11. CONTROLLING OFFICE NAME AND ADDRESS ONRR, University of California 553 Evans Hall University of California, Berkeley, CA 94720		12. REPORT DATE July 1974 13. NUMBER OF PAGES 47
14. MONITORING AGENCY NAME & ADDRESS*(if different from Controlling Office)*		15. SECURITY CLASS. *(of this report)* UNCLASSIFIED 15a. DECLASSIFICATION/DOWNGRADING SCHEDULE

16. DISTRIBUTION STATEMENT *(of this Report)*

17. DISTRIBUTION STATEMENT *(of the abstract entered in Block 20, if different from Report)*

18. SUPPLEMENTARY NOTES

19. KEY WORDS *(Continue on reverse side if necessary and identify by block number)*

Finite elements; Dynamics; Plasticity; Axisymmetric; Large displacements; Lagrangian formulation

20. ABSTRACT *(Continue on reverse side if necessary and identify by block number)*

see reverse

DD FORM 1 JAN 73 1473 EDITION OF 1 NOV 65 IS OBSOLETE
S/N 0102-014-6601

UNCLASSIFIED